Journal of Materials Chemistry A

ROYAL SOCIETY OF CHEMISTRY

REVIEW

View Article Online
View Journal | View Issue

Check for updates

Cite this: J. Mater. Chem. A, 2026, 14, 12566

Carbon material-driven photothermal CO_2 reduction for catalyzing a circular carbon economy

Yanlin Liao,[ab] Shuangjun Li,[c] Yan Xie,[ab] Hao Wen,[d] Bo Weng,[ef] Hao Sun*[d] and Xiangzhou Yuan*[ab]

Photothermal CO_2 reduction has attracted increasing attention as a promising and practical strategy to simultaneously mitigate climate change and catalyze a circular carbon economy. Carbon materials, possessing abundant pore structures, broad-spectrum light absorptions, accessible electron transport pathways, and adjustable electronic structures, emerge as particularly attractive catalysts for photothermal CO_2 reduction. However, concerted efforts need to reveal photothermal-coupling mechanisms, multifunctional roles, and accurate design principles of carbon materials for catalyzing photothermal CO_2 reductions. In this review, photo-generated and thermo-driving forces with their synergistic effects are comprehensively addressed using carbon-based catalysts to establish mechanistic frameworks for photothermal CO_2 reduction as well as propose a potential solution for key existing challenges. Multifaceted roles of carbon materials for catalyzing photothermal CO_2 reduction are discussed from the perspectives of active, functional, and regulatory phases and also product selectivity. Artificial intelligence (AI)-empowered modification strategies, including heteroatom doping, interface engineering, and morphological/structural design, are critically reviewed to elucidate their contributions for constructing efficient photothermal CO_2 reduction systems. Moreover, considering both environmental and economic benefits, both life-cycle and techno-economic assessments (LCA & TEA) are performed for comprehensively evaluating the commercial feasibility of carbon-based photothermal CO_2 reduction, shedding valuable lights on both academic and governmental communities. Finally, future prospects of carbon material-driven photothermal CO_2 reduction reactions are proposed to solve main challenges and accelerate related commercial deployments, which are beneficial to mitigating climate change and catalyzing a circular carbon economy.

Received 5th December 2025
Accepted 9th February 2026

DOI: 10.1039/d5ta09948j

rsc.li/materials-a

Open Access Article. Published on 10 2026. Downloaded on 17.05.26 9:18:50.
This article is licensed under a Creative Commons Attribution-NonCommercial 3.0 Unported Licence.

1 Introduction

The excessive use of fossil fuels has led to a dramatic rise in atmospheric CO_2 concentration (even up to 420 ppm),[1] strongly intensifying climate change including ocean acidification and extreme weather.[2] Because of that, CO_2 is widely considered as the key greenhouse gas contributing to climate change, and concerted efforts urgently need to be made for sustainably transforming CO_2 into value-added products (*i.e.*, methanol, ethylene, and ethanol), which is beneficial to achieving both environmental sustainability and energy crisis solidification.[3,4] As shown in Table 1, numerous strategies have been explored to convert CO_2 into fuels and value-added chemicals,[5–10] and photocatalytic CO_2 reduction has attracted widespread attention, mainly because it directly harnesses solar energy under mild conditions without the need for external electricity input.[11–13] Current photocatalytic CO_2 reduction applications are still immature, particularly owing to limited utilization of the solar spectrum, rapid recombination of photogenerated charge carriers, and low space–time yields.[14,15] Thus, photocatalysis alone is insufficient to achieve high-performance CO_2 conversion, and photothermal catalytic CO_2 reduction, as a photo-induced coupled strategy, has consequently emerged as a promising approach. The coupling of photonic and thermal effects not only lowers the activation energy of CO_2 conversion but also accelerates mass transport and charge migration, thereby achieving higher catalytic activity and selectivity than those of either photocatalysis or thermocatalysis alone.[16,17] Recent studies and reviews have highlighted that the advantages of photothermal catalysis in CO_2 reduction primarily lie in

[a]Key Laboratory of Energy Thermal Conversion and Control of Ministry of Education, School of Energy and Environment, Southeast University, Nanjing 210096, China. E-mail: yuanxz@seu.edu.cn

[b]Key Laboratory of Functional Polymers for Sustainability of Jiangsu, School of Energy and Environment, Southeast University, Nanjing 210096, China

[c]Department of Chemical and Biological Engineering, Korea University, 145 Anam-ro, Seongbuk-gu, Seoul 02841, South Korea

[d]State Key Laboratory for Development and Utilization of Forest Food Resources, Institute of Chemical Industry of Forest Products, Chinese Academy of Forestry, Nanjing 210042, China. E-mail: sunhao@icifp.com

[e]State Key Laboratory of Advanced Environmental Technology, Institute of Urban Environment, Chinese Academy of Sciences, Xiamen 361021, China

[f]University of Chinese Academy of Sciences, 19A Yuquan Road, Beijing 100049, China

This journal is © The Royal Society of Chemistry 2026

Open Access Article. Published on 10 2026. Downloaded on 17.05.26 9:18:50.
This article is licensed under a Creative Commons Attribution-NonCommercial 3.0 Unported Licence.

Table 1 Comparison of typical single and photo-driven coupled CO_2 reduction technologies

Categories	Catalytic technologies	Advantages	Disadvantages
Single catalytic technologies	Electrocatalysis	• Ambient-condition CO_2 conversion with tunable product output • Scalable modular reactors	• High energy input and complex system cost • Low CO_2 solubility in aqueous media • Short catalyst lifetime under continuous operation
	Thermocatalysis	• High CO_2 conversion rates and fast reaction kinetics • Compatibility with industrial-scale continuous processes	• High-temperature energy demand • Catalyst deactivation *via* coking and sintering during prolonged operation
	Photocatalysis	• Low external energy demand with solar-driven operation • CO_2 conversion with controllable output under green and mild conditions	• Limited solar absorption • Rapid photogenerated charge recombination • Relatively low overall conversion efficiency
Photo-driven coupled catalytic technologies	Photoelectrocatalysis	• High product yield and selectivity • Integration of solar energy utilization and electrochemical control	• Poor long-term stability of photoelectrodes • Complex system architecture with scaling challenges
	Photothermal catalysis	• Enhanced solar energy utilization • High product yield and CO_2 conversion rates under moderate reaction conditions • Synergistic thermal and photochemical effects	• Challenges in thermal management and accurate temperature monitoring • Scalability limitations due to strong dependence on light intensity

solar energy-driven upcycling systems in a renewable and practical manner and high feasibility for widespread deployment.[18,19]

Carbon materials have recently attracted broad interest in photothermal CO_2 reduction. Their intrinsic physicochemical properties, including abundant pore structures,[20] broad-spectrum light absorption,[21] accessible electron transport pathways,[22] and adjustable electronic structures, provide a favourable platform for photothermal CO_2 reduction. The low cost and renewability of certain carbon materials, such as biomass-derived carbons, further enhance their potential for sustainable catalyst development.[31] Driven by these advantages, significant progress has been made in developing diverse carbon-based photothermal catalysts (Fig. 1a), including carbon quantum dots (CDs), carbon nanotubes (CNTs), graphene derivatives, hierarchical carbon nanocages (hCNCs), metal–organic framework (MOF)-derived carbons, biomass-derived carbons, and other porous carbons.[29,32–37] Fig. 1b and c show a continuous increase in publications related to photo-driven carbon-based catalysts, with the proportion of carbon-based catalysts in photothermal systems remaining above 30% in recent years. These rapid developments highlight the need for a systematic assessment of recent advances to support the rational development of carbon-based photothermal catalysts. Although several reviews have discussed recent progress in photothermal CO_2 reduction or examined the catalytic applications of carbon materials, the two subjects have largely been addressed separately rather than in an integrated manner.[38–46] For example, Amoo *et al.* discussed the influence of carbon-based physicochemical properties on CO_2 conversion through catalytic routes and only briefly mentioned photothermal catalysis.[47] Thus, there is still a lack of comprehensive reviews that systematically summarize photothermal-coupling mechanisms, multifunctional roles, and accurate design principles of carbon-based photothermal CO_2 reduction. As research in both photothermal catalysis and carbon material engineering continues to expand rapidly, consolidating these advances into a comprehensive framework has become increasingly necessary.

In this context, we organize recent advances in carbon-based photothermal CO_2 reduction through a comprehensive and systematic manner. The mechanistic scheme was constructed based on representative carbon-based catalysts to elucidate the fundamental reaction principles and summarize the major scientific challenges of photothermal CO_2 reduction. Building on the intrinsic advantages of carbon materials, the multifaceted functions were then discussed to mitigate the existing challenges. By identifying the limitations of carbon materials, the modification strategies were evaluated, with AI-empowered approaches further supporting the construction of efficient photothermal CO_2 reduction systems. Furthermore, the environmental benefits and economic feasibility of carbon-based photothermal CO_2 reduction systems are performed through LCA and TEA, offering quantitative benchmarks for commercial assessment and decision-making. Finally, future research directions of carbon material-driven photothermal CO_2 reductions are proposed, with the aim of accelerating the transition of this technology toward practical deployment, thereby supporting climate mitigation efforts and the development of a circular carbon economy.

Open Access Article. Published on 10 2026. Downloaded on 17.05.26 9:18:50.
This article is licensed under a Creative Commons Attribution-NonCommercial 3.0 Unported Licence.

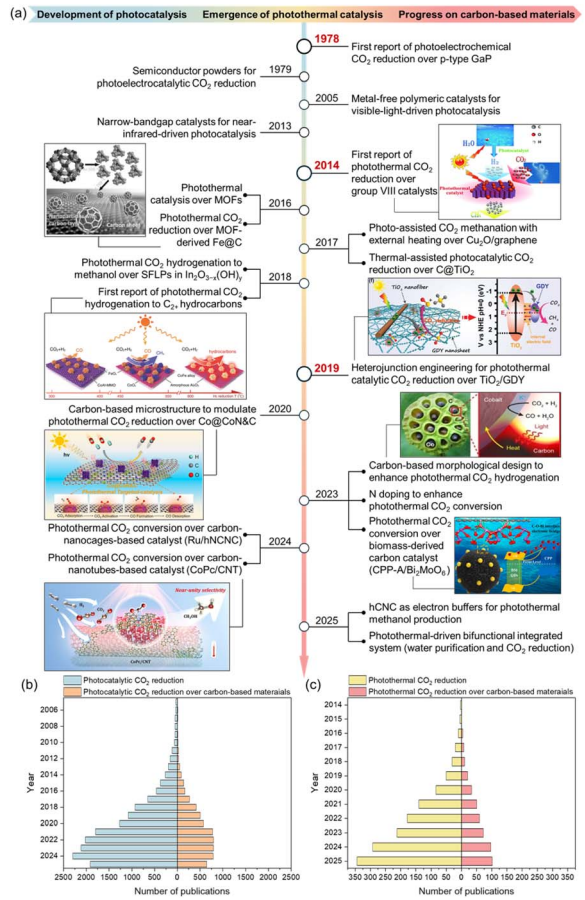

Fig. 1 (a) The timeline of key developments from photocatalytic to photothermal CO_2 reduction on carbon materials. Reproduced with permission.[23] Copyright 2014, John Wiley & Sons. Reproduced with permission.[24] Copyright 2016, John Wiley & Sons. Reproduced with permission.[25] Copyright 2018, John Wiley & Sons. Reproduced with permission.[26] Copyright 2019, John Wiley & Sons. Reproduced with permission.[27] Copyright 2020, American Chemical Society. Reproduced with permission.[28] Copyright 2023, John Wiley & Sons. Reproduced with permission.[29] Copyright 2023, American Chemical Society. Reproduced with permission.[30] Copyright 2024, John Wiley & Sons. The number and proportion of publications related to (b) photocatalytic and (c) photothermal catalytic CO_2 reduction over whole catalysts and carbon-based catalysts (data for the graphs were obtained from the Web of Science Core Collection).

2 Basic principles of carbon-driven photothermal CO_2 reduction

The fundamental objective of photothermal CO_2 reduction is to utilize light and heat energy as driving forces for CO_2 activation, particularly for weakening the C=O bond (bond energy of about 750 kJ mol^{-1}) and enabling the formation and transformation of key intermediates.[48,49] Understanding these driving forces is essential for elucidating the photothermal synergistic pathways of CO_2 reduction.

2.1 Driving forces of photothermal CO_2 reduction

From the perspective of photo-induced electronic driving, the incident light generates charge carriers or hot carriers that

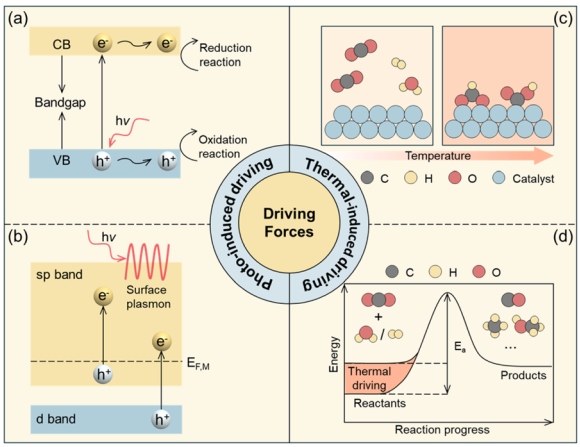

Fig. 2 Driving forces of photothermal CO_2 reduction: (a) photogenerated carriers, (b) plasmon-induced hot carriers, (c) thermal-driven intermolecular collisions and (d) thermal-induced increase in the population of electronic states, where $E_{F,M}$ denotes the Fermi level.

supply the necessary redox potential for CO_2 activation. In semiconductor-based systems, when photons with energies equal to or exceeding the bandgap are absorbed, electrons in the valence band (VB) are excited into the conduction band (CB), generating electron–hole pairs. These carriers migrate to the catalyst surface, where they participate in reduction and oxidation processes (Fig. 2a).[50–52] In metal nanostructure systems with localized surface plasmon resonance (LSPR) effects, the nonradiative decay of photon-induced collective oscillations excites a portion of electrons above the Fermi level, forming high-energy hot electrons and holes (Fig. 2b). These carriers are directly injected into reactant molecules or semiconductor bands, thereby accelerating surface reaction kinetics.[53–55]

Meanwhile, thermal energy plays an equally indispensable role in photothermal catalysis. The temperature rise induced by photo-to-thermal conversion or external heating enhances the kinetics of reactant molecules, increasing the frequency of effective intermolecular collisions (Fig. 2c).[56] Furthermore, the increase in temperature alters the energy distribution, shifting the Boltzmann population of molecules toward high energy states (Fig. 2d);[57] the temperature rise accelerates the diffusion of reactants and intermediates, improving mass transport efficiency.[58]

In most photothermal systems, photo-to-thermal conversion contains the principal source of thermal energy. Compared with external heating, photo-induced heat enables precise modulation of the local temperature at active sites under illumination, thereby accelerating surface reactions. The mechanisms of photo-to-thermal conversion are classified into three main categories. (1) In semiconductor systems, a fraction of photogenerated carriers recombine through electron-phonon interactions, releasing their excess energy nonradiatively to the lattice and producing localized heating.[59–61] (2) In plasmonic materials, the photoexcited high-energy hot carriers undergo rapid electron-phonon scattering, during which their energy is transferred to lattice vibrations, resulting in instantaneous local

This journal is © The Royal Society of Chemistry 2026

Open Access Article. Published on 10 2026. Downloaded on 17.05.26 9:18:50.
This article is licensed under a Creative Commons Attribution-NonCommercial 3.0 Unported Licence.

heating.[62–64] (3) In carbon materials, the abundant π–π conjugated structures and delocalized electron systems endow them with broad-spectrum absorption capability. π–π* transitions generate excited electrons that relax through vibronic coupling and dissipate energy as heat, producing localized thermal fields.[65–67] This electron-vibration energy dissipation mechanism underpins the efficient photothermal response of carbon materials in CO_2 reduction. Moreover, as for carbon materials, beyond serving as photo-to-thermal converters, they can act as supports for semiconductor and plasmonic components, which enable efficient coupling of photogenerated charges, hot-carrier processes, and local photothermal heating, resulting in an integrated catalytic platform.

2.2 Photothermal synergistic pathways of CO_2 reduction: representative carbon material-driven systems

Photothermal catalysis is not a simple superposition of photo and thermal driving forces but a process where their synergy defines the catalytic essence. Three cooperative modes are illustrated using carbon materials as representative systems to highlight their mechanistic differences and functional characteristics.

Photo-induced thermal catalysis refers to processes in which illumination primarily induces photo-to-thermal conversion or hot-carrier excitation to drive thermally dominated surface reactions (Fig. 3a). Mechanistically, this mode is essentially a thermal catalysis process triggered by light. For example, a Ru–ZrO_2/C catalyst was reported to exhibit similar CH_4 yields under both photothermal and thermal conditions at comparable surface temperatures, confirming that the catalytic process was dominated by photo-to-thermal heating, where light served primarily as a thermal source to initiate CO_2 methanation.[68]

Thermal-assisted photocatalysis, by contrast, is primarily governed by photocatalytic processes, with heat serving as a synergistic factor. In this mechanism, photocatalysts absorb photons to generate carriers, which can be effectively transferred *via* carbon-based components to active sites, where carriers participate in CO_2 reduction and hydrogen-donor oxidation, respectively (Fig. 3b). Moderate temperature elevation, either from photothermal heating or external sources, promotes charge separation, accelerates surface reaction kinetics, and improves mass transport, collectively boosting the activity and selectivity. Research on CO_2 reduction over carbon@TiO_2 composites revealed that photogenerated carriers in TiO_2 drove the redox reactions, while local photothermal heating by the carbon layer further enhanced carrier mobility and reaction kinetics.[69] Wang *et al.* investigated In_2O_3@carbon catalysts and found that CO production rates under illumination significantly exceeded those obtained in the dark at comparable surface temperatures. The gap widened at higher light intensities, demonstrating that nonthermal effects dominated under strong illumination.[36]

Photothermal synergistic catalysis represents a major integrated mode, where photochemical and thermochemical pathways coexist and operate cooperatively. Under illumination, catalysts simultaneously convert light into localized heat and generate charge carriers (Fig. 3d and e). The photogenerated electrons and holes open new pathways for CO_2 reduction, while the thermal field drives the acceleration of the thermocatalytic process.[70] Yang *et al.* reported that the CH_4 formation rate of RuCo/ZrO_2 fibre cotton increased with light intensity, indicating that the reaction was primarily governed by photothermal effects. Meanwhile, the lower apparent activation energy observed under photo conditions, compared with purely thermal catalysis, confirmed that the photothermal system followed an alternative reaction pathway with reduced kinetic barriers.[71] Fig. 3c illustrates a representative mode in which carbon-based catalysts participate in photothermal synergistic catalysis. The carbon component not only enhances the surface temperature through efficient light-to-heat conversion but also serves as an electron transport channel that facilitates charge migration and transfer across the reaction interface.[33]

It is worth noting that, in ideal cases, integrating semiconductor catalysts that absorb ultraviolet/visible light with carbon materials possessing near-infrared absorption can yield full-spectrum photothermal systems while simultaneously mitigating the annihilation of photogenerated charge carriers. However, in practice, there may be competition between photon absorption for photocarrier generation and photo-to-thermal conversion. Wang *et al.* found that excessive graphene oxide (GO) content in GO/CoS_2/microtubule g-C_3N_4 (TCN) composites led to excessive photon capture by GO, reducing the light absorption and excitation of TCN and consequently suppressing photocarrier generation.[72] Therefore, catalytic composition should be identified to balance photocarrier production and photothermal heating. This balance is closely linked to a synergy optimal temperature range, because an overly thermal dominated mechanism reduces the role of photocarriers, while an excessive photo effect may not provide sufficient thermal driving for kinetically demanding steps. Tuning the relative proportion and coupling of carbon and semiconductor components are thus essential to maximize the cooperative benefit of photothermal synergistic processes for CO_2 conversion.

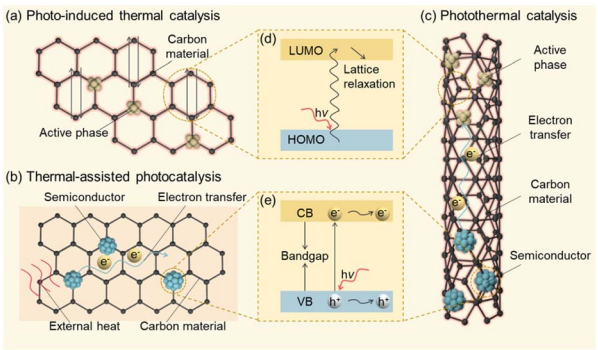

Fig. 3 Three cooperative modes for photothermal CO_2 reduction: (a) photo-induced catalysis, (b) thermal-assisted photocatalysis, and (c) photothermal synergistic catalysis. (d) Photo-to-thermal process on carbon materials in photo-induced and photothermal synergistic catalysis, where the HOMO and LUMO denote the highest occupied and lowest unoccupied molecular orbitals, respectively. (e) Photochemical process on semiconductors in thermal-assisted photocatalysis and photothermal synergistic catalysis.

Open Access Article. Published on 10 2026. Downloaded on 17.05.26 9:18:50.
This article is licensed under a Creative Commons Attribution-NonCommercial 3.0 Unported Licence.

2.3 Challenges in photothermal CO_2 reduction

Based on the understanding of the photothermal synergistic mechanism discussed above, although significant progress has been achieved in photothermal CO_2 reduction in recent years, several key challenges still limit its reaction efficiency and stability.

(1) Insufficient adsorption and activation sites for CO_2 molecules

CO_2 molecules exhibit strong chemical inertness, making their adsorption and bending activation on the catalyst surface difficult.[73] Since most photothermal reactions proceed under mild conditions, insufficient light-induced heating and photogenerated carriers cannot provide energy required to active CO_2 molecules, leading to sluggish formation of a CO_2^* intermediate.

(2) Difficulties in carrier separation and transport

The efficient separation and migration of photoinduced carriers are essential to drive surface reduction reactions in photothermal CO_2 reduction.[74] However, these carriers tend to recombine rapidly after excitation by light, and elevated temperatures may further accelerate recombination under photothermal conditions.

(3) Limited photo-to-thermal conversion efficiency

Moderate photo-to-thermal conversion is the prerequisite for maintaining the reaction temperature.[75] However, some catalytic systems only absorb narrowband radiation, resulting in a low utilization rate of the solar spectrum. Specifically, the radiative heat loss reduces the effective temperature rise, making it difficult to maintain an optimal reaction temperature range required by reaction kinetics and thermodynamics solely under solar irradiation.

(4) Challenges in directional conversion of CO_2 to products

Photothermal CO_2 reduction generally involves multistep proton–electron coupling reactions with complex intermediates and small energy differences among competing pathways, which leads to strong reaction competition.[76] The transformation between various intermediates is highly sensitive to surface structure, which is capable of significantly altering the product distributions.

Overall, photothermal CO_2 reduction systems still face significant challenges in CO_2 activation, carrier separation and migration, energy conversion, and reaction selectivity. The introduction of carbon materials with tunable structural and electronic properties into catalytic systems is expected to address these limitations by enabling the synergistic regulation of light, heat, electrons, and reaction pathways, thereby promoting efficient and selective photothermal CO_2 reduction.

3 Roles and mechanistic functions of carbon materials for high-performance photothermal CO_2 reduction

In photothermal CO_2 reduction systems, carbon materials play multifaceted roles (Fig. 4). Their abundant pore structures, broad-spectrum light absorption, accessible electron transport pathways, and adjustable electronic structure enable the coordinated regulation of the photothermal CO_2 reduction process.

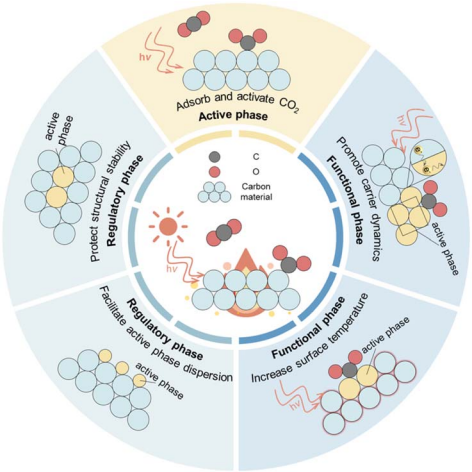

Fig. 4 Roles of carbon materials in photothermal CO_2 reduction.

3.1 Roles of carbon materials in photothermal CO_2 reduction

Depending on the function of carbon materials within the catalytic architecture, they are categorized into three representative phases of active phase, functional phase, and regulatory phase.

3.1.1 Active phase for CO_2 adsorption and activation. The adsorption of CO_2 molecules on the catalyst surface represents the first and essential step in photothermal CO_2 reduction. The CO_2 adsorption capability of a catalyst determines its potential for subsequent conversion to target products. The sites responsible for CO_2 adsorption and activation directly participate in product formation and are therefore denoted as active phases. Table 2 summarizes recent photothermal CO_2 reduction systems in which carbon materials function as active phases.

CO_2 adsorption and activation ability of carbon materials primarily originates from their intrinsic structural characteristics. Specifically, the porous architectures and large surface areas substantially enhance the contact probability and adsorption capacity of CO_2 molecules. Microporous carbons with cumulative pore volumes under 0.8 nm are the most favourable. Such narrow pores are slightly larger than twice the kinetic diameter of CO_2, enabling an optimal confinement environment, which leads to enhanced interactions between CO_2 molecules and pore walls.[77–79] However, for CO_2 reduction processes, catalytic conversion is not only determined by adsorption efficiency. More importantly, mass transfer of reactants and products, accessibility of active phases, and the residence time of key intermediates play critical roles, especially under continuous-flow and high-temperature conditions relevant to photothermal catalysis. In this context, mesopores with sizes between 2 and 50 nm are more favourable for photothermal-driven catalytic CO_2 reduction, as they provide efficient transport pathways that reduce diffusion limitations

 This journal is © The Royal Society of Chemistry 2026

Open Access Article. Published on 10 2026. Downloaded on 17.05.26 9:18:50.
This article is licensed under a Creative Commons Attribution-NonCommercial 3.0 Unported Licence.

Table 2 Recent applications of carbon materials as active phases in photothermal CO_2 reduction

Types of carbon-based active phases	Catalysts	Reactants	Reaction conditions	Product	Production rate (μmol g^{-1} h^{-1})	Selectivity (%)
Graphene-based material	Cu_2O/graphene[34]	CO_2 + H_2 (1 : 4)	300 W Xe lamp + 250 °C, Cu content: 0.56 mg, batch reactor, 1.3 bar	CH_4	14 930	99
	TiO_2–graphene[83]	CO_2 + H_2O	300 W Xe lamp (0.438 W cm^{-2}), 116.4 °C, 50 mg, batch reactor	CO CH_4	5.2 26.7	16.3 83.7
	NiO/Ni-graphene[84]	CO_2 + H_2	300 W Xe lamp + 200 °C, Ni content: 9.2 mg, batch reactor, 1.3 bar	CH_4	642.66	—
	Bi_2MoO_6/rGO[85]	CO_2 + H_2O	300 W Xe lamp with AM 1.5 filter, 68.0 °C, batch reactor	CO	186.87	100
	Bi_2MoO_6–I QDs/rGO[86]	CO_2 + H_2O	300 W Xe lamp with AM 1.5 filter (0.6 W cm^{-2}), 74.6 °C, 20 mg, batch reactor	CO	30.15	100
Biomass-derived carbon material	CPP-A/Bi_2MoO_6 QDs[29]	CO_2 + H_2O	300 W Xe lamp with AM 1.5 filter, 100 °C, batch reactor	CO	61.44	100
	BCF/Bi_2MoO_6 (ref. 87)	CO_2 + H_2O	300 W Xe lamp with AM 1.5 filter (1.5 W cm^2), 176.4 °C, 15 mg, batch reactor	CO	165	100
	g-C_3N_4@CPP/ BiOClBr-O_V[88]	CO_2 + H_2O	300 W Xe lamp, 130 °C, 15 mg, batch reactor	CO	22.92	99
MOF-derived metal@ carbon material	Fe@C[24]	CO_2 + H_2 (1 : 1)	300 W Xe lamp, 481 °C, 60 mg, batch reactor	CO	26 120	>98
	Fe@C/Ni_2P[89]	CO_2 + H_2O	350 W LED lamp (λ = 420 nm) + 200 °C, 20 mg, batch reactor	CO	179.9	96.9
	Co@NC[90]	CO_2 + H_2 (1 : 1)	300 W Xe lamp (3 W cm^{-2}), 378 °C, batch reactor	CO	536 700	92.6
Porous carbon material	C@TiO_2 (ref. 69)	CO_2 + H_2O	300 W Xe lamp, 100 mg, batch reactor, 1 bar	CH_4	4.2	31.6
	Co@CoN&C[27]	CO_2 + H_2 (1 : 1)	300 W Xe lamp, ~518 °C, 50 mg, batch reactor, ~0.55 bar	CO	132 000	91.1

and expose excellent proportion of accessible active phases.[80,81] Moreover, recent studies have shown that hierarchical porous materials that integrate micropores, mesopores, and macropores into a cooperative multiscale structure synergistically combine strong CO_2 adsorption with enhanced mass transfer, leading to significant performance enhancement of photothermal CO_2 conversion.[82]

Beyond pore structure effects, electronic characteristics of carbon frameworks further contribute to CO_2 adsorption and activation. Specifically, π–π conjugated carbon frameworks provide delocalized π-electron clouds that interact weakly with CO_2 molecules, thereby enhancing their adsorption affinity. The research on core–shell Co@CoN&C revealed that the CO_2 adsorption capacity was closely correlated with the carbon shell content.[27] Wang *et al.* demonstrated that hybrid carbon@TiO_2 hollow spheres exhibited enhanced CO_2 adsorption due to their abundant porosity and high surface area, whereas the π–π conjugation within the carbon spheres further reinforced CO_2 binding.[69] Yu *et al.* investigated the CO_2 adsorption behaviour on a TiO_2/graphdiyne heterostructure and found that the acetylenic bonds in graphdiyne served as preferential active sites for CO_2 activation and subsequent photoreduction, thereby enhancing the overall CO_2 reduction efficiency.[26]

However, the intrinsic physicochemical properties of carbon-based catalysts are often insufficient to ensure efficient chemical activation of CO_2. It was reported that, in a Co@carbon nanotube (CN), CN structures only enhanced the localized concentration of CO_2 near the catalyst by physical adsorption, while the chemical adsorption on Co sites further promoted the CO_2 reduction process.[91] Therefore, beyond relying on the intrinsic adsorption and enrichment ability of carbon materials, structural and electronic modifications are necessary to enhance their capacity for CO_2 adsorption and activation.

3.1.2 Functional phase for carrier dynamic promotion and photo-induced heat effect enhancement. In photothermal CO_2 reduction systems, some carbon materials do not directly serve as the main active sites for CO_2 adsorption and activation. However, they play important auxiliary roles in facilitating the catalytic process by mediating carrier behaviour and generating localized heating, which were denoted as functional phases. Table 3 summarizes recent photothermal CO_2 reduction systems in which carbon materials were employed as functional phases.

(1) Promote the generation and transport of carriers

As functional phases, the role of carbon-based functional phases lies in constructing efficient charge-transport networks that enable rapid migration of electrons and holes to the reaction interface, where they participate in redox processes. Charge transport capability of carbon materials originates from their intrinsic electronic structures. The conductive sp^2-hybridized carbon framework provides continuous pathways for electron motion, while the π–π conjugated system allows charge

Open Access Article. Published on 10 2026. Downloaded on 17.05.26 9:18:50.
This article is licensed under a Creative Commons Attribution-NonCommercial 3.0 Unported Licence.

Table 3 Recent applications of carbon materials as functional phases in photothermal CO_2 reduction

Types of carbon-based functional phase	Catalysts	Reactants	Reaction conditions	Product	Production rate ($\mu mol\ g^{-1}\ h^{-1}$)	Selectivity (%)
CDs-based materials	Pt/30-CDs/Zr/MOF[34]	$CO_2 + H_2$ (1 : 4)	300 W Xe lamp (1.2 W cm^{-2}) + 300 °C, 160 mg, continuous-flow reactor, 1 bar	CO	22 520	99
	Bi-CDs/LDH[95]	$CO_2 + H_2O$	300 W Xe lamp with AM 1.5 G filter, 109 °C, 50 mg, batch reactor, 100 kPa	C_2	3.52	36.6
CNTs-based materials	CdS/CNT/CoPc[35]	CO_2 + TEOA	150 W Xe lamp with AM 1.5 G-filter (0.216 W cm^{-2}), 50 °C, 1 mg, continuous-flow reactor	CO	3100	100
	CoPc/CNT[33]	$CO_2 + H_2$ (1 : 3)	1000 W Xe lamp (2.0 W cm^{-2}), 250 °C, 15 mg, batch reactor, 40 bar	CH_3OH	2400	99
	Co@CN[87]	$CO_2 + H_2$	300 W UV-Xe lamp (2.5 W cm^{-2}) + 250 °C, 15 mg, batch reactor, 10 bar	CH_4	199 400	99.4
Graphene-based materials	GO/CoS_2/TCN[94]	$CO_2 + H_2O$	300 W Xe lamp, 165.3 °C, 50 mg, batch reactor, 0.7 bar	CO CH_4	28.74 12.05	70.5 29.5
	Fe@(N)C[99]	$CO_2 + H_2$ (1 : 1)	300 W Xe lamp (0.12 W cm^{-2}, 330–800 nm) + 245 °C, 40 mg, batch reactor, 1.4 bar	CO	75.2	100
hCNCs-based materials	Ru/hNCNC[37]	$CO_2 + H_2$ (1 : 1)	300 W Xe lamp (2.4 W cm^{-2}), ~410 °C, 5 mg, continuous-flow reactor	CO	376 000	91.4
	In_2O_3/hCNC[107]	$CO_2 + H_2$ (1 : 3)	300 W Xe lamp (0.4 W cm^{-2}) + 350°C, 25 mg, continuous-flow reactor, 28 bar	CH_3OH	6127	20.5
MOF-derived metal@carbon materials	ZnSe–CdSe@NC FC[108]	$CO_2 + H_2O$	300 W Xe lamp (400–1100 nm), 91 °C, 5 mg, batch reactor	CO	31.62	>90
	Ni@C100	$CO_2 + H_2$ (1 : 4)	300 W Xe lamp (0.12 W cm^{-2}), 25 mg, batch reactor, 5 bar	CH_4	488 000	100
	Rb/In@C[38]	$CO_2 + H_2$ (1 : 4)	300 W Xe lamp, 254 °C, 30 mg, continuous-flow reactor, 1 bar	CO	53 000	100
	Ru–ZrO_2/C[70]	$CO_2 + H_2$ (1 : 4)	300 W Xe lamp (2.614 W cm^{-2}), 370 °C, 10 mg, batch reactor	CH_4	504 100	98.9
	Co/NC[109]	$CO_2 + H_2$ (1 : 4)	300 W Xe lamp (0.0382 W cm^{-2}), Fresnel lens (1.55 W cm^{-2}), 310 °C, 100 mg, continuous-flow reactor, 1 bar	CH_4	21 600	94.3
	Co/NC[110]	$CO_2 + H_2$ (1 : 4)	300 W Xe lamp (5.2 W cm^{-2}, 300–2500 nm), 300 °C, 100 mg, batch reactor, 2 bar	CH_4	758 000	99.6
	CoOx@C[106]	$CO_2 + H_2$	Lamp + 200 °C, 100 mg, continuous-flow reactor, 1 bar	CH_4	2890	96.15
Other porous carbon materials	Cu–Cu_2O–CuS@C[111]	$CO_2 + H_2O$	300 W Xe lamp (0.171 W cm^{-2}, 400–1100 nm), 190 °C, 5 mg, batch reactor	CO	22.6	88.1
	K^+–Co–C[31]	$CO_2 + H_2$ (1 : 1)	300 W Xe lamp (2.8 W cm^{-2}), 440 °C, 5 mg, continuous-flow reactor	CO	758 000	99.8
	oCB/Cu/ZnO/Al_2O_3 (ref. 39)	$CO_2 + H_2$ (1 : 3)	300 W Xe lamp (2.8 W cm^{-2}), 305 °C, batch reactor, 8 bar	CH_3OH	4910	64.7
	Na–Co@C[112]	$CO_2 + H_2$ (1 : 5)	1000 W Xe lamp with AM 1.5 G filter (2.4 W cm^{-2}), 235 °C, 75 mg, batch reactor, 2.8 bar	CO CH_4 C_2H_5OH C_{2+}	— — — —	4.8 50.2 6.5 38.5

This journal is © The Royal Society of Chemistry 2026

Open Access Article. Published on 10 2026. Downloaded on 17.05.26 9:18:50.
This article is licensed under a Creative Commons Attribution-NonCommercial 3.0 Unported Licence.

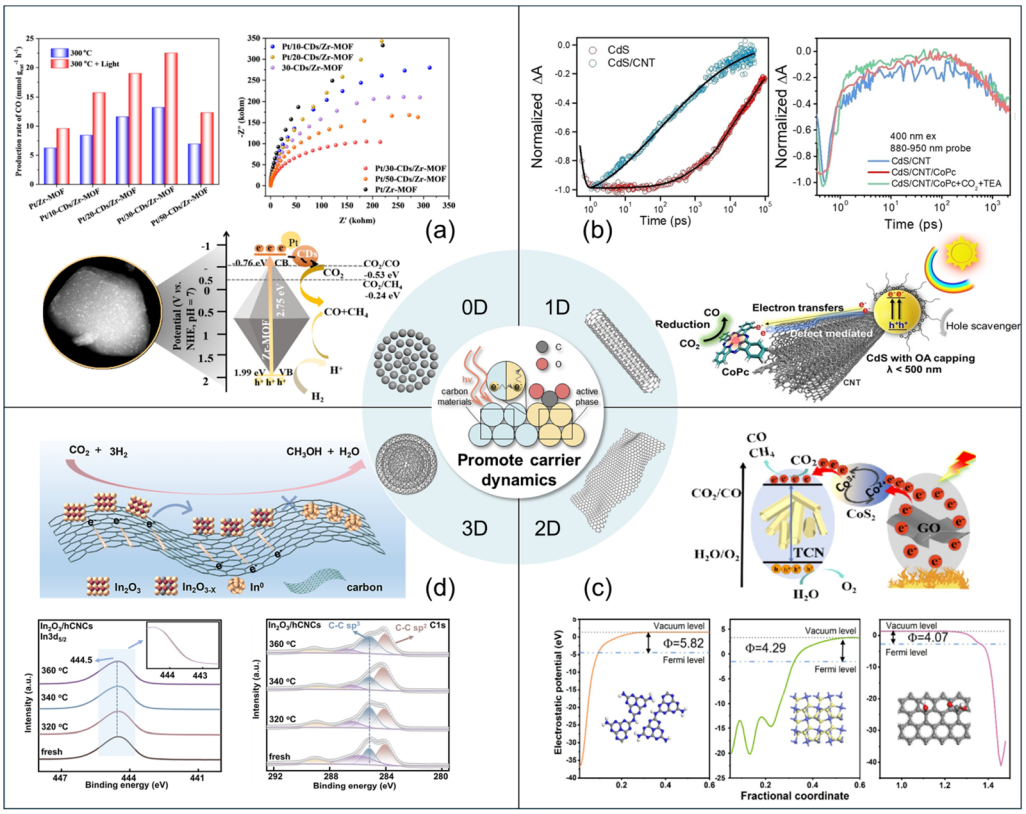

Fig. 5 Carbon-based functional phases for promoting the electron generation and transfer of carriers: (a) effect of CD content on carrier generation and transfer efficiency in Pt/CDs/Zr-MOF. Reproduced with permission.[32] Copyright 2025, Elsevier. (b) Effect of CNTs on carrier separation and transfer in CdS/CNT/CoPc. Reproduced with permission.[33] Copyright 2023, John Wiley & Sons. (c) Effect of graphene on carrier generation in GO/CoS_2/TCN. Reproduced with permission.[99] Copyright 2025, Elsevier. (d) Effect of hCNCs on carrier transfer in In_2O_3/hCNCs. Reproduced with permission.[72] Copyright 2025, American Chemical Society.

migration through delocalized orbitals, reducing energy dissipation and limiting carrier recombination.[92–94]

CDs, as zero-dimensional nanomaterials, have emerged as highly promising materials for photothermal catalysis.[95] On the one hand, CDs can generate charge carriers under light irradiation. On the other, their low-dimensional nature facilitates overcoming carrier migration bottlenecks in CO_2 reduction, as dimensional confinement effectively shortens carrier migration pathways.[96,97] In the Pt/CDs/Zr-MOF system, CDs acted as both local electron donors and acceptors (Fig. 5a). As donors, they supplied additional electrons to the catalytic reaction, while as acceptors, they facilitated electron transfer from the conduction band of Zr-MOF to their surface, thereby enhancing charge separation.[32] Yu *et al.* reported that in the Bi-CDs/layered double hydroxide (LDH) heterojunction, CDs functioned as electron reservoirs that captured electrons from LDH and released them on demand to the reaction interface, dynamically regulating interfacial charge transfer and maintaining a balance between electron accumulation and consumption to improve catalytic activity.[98]

The unique tubular architecture of one-dimensional CNTs endows them with superior axial electron mobility, which greatly facilitates the efficient separation of photogenerated charge carriers.[100] In the CdS/CNT/cobalt phthalocyanine (CoPc) ternary hybrid catalyst, CNTs serve as electron channels, transferring electrons from CdS to CoPc active sites and increasing the CO production rate from 0.1 to 3.1 μmol h^{-1} (Fig. 5b).[33] Beyond transporting photoinduced charge carriers, CNTs also mediate LSPR induced hot-carrier generation and transfer in photothermal processes. The carbon shell in Co@CN catalysts has been reported to enhance the LSPR effect of Co nanoparticles, promoting the generation of hot carriers and therefore facilitating the activation of adsorbed molecules.[91,101]

Most studies have consistently reported that two-dimensional graphene, due to its zero bandgap, cannot be directly photoexcited to generate charge carriers for photocatalytic reactions.[102] Nevertheless, some studies have demonstrated that graphene can be modulated to provide electrons when employed as a functional phase in photothermal CO_2 reduction. Szalad *et al.* found that N-doped defective graphene can absorb ultraviolet light to generate charge carriers, while the Fe clusters acted as recombination centres that induced local heating.[103] Zeng *et al.* measured the work functions of GO/CoS_2/TCN and proposed that electrons spontaneously migrate from GO to CoS_2 to TCN (Fig. 5c).[99]

Three-dimensional hCNCs have been demonstrated to function as effective electron buffers in photothermal CO_2 hydrogenation. Wang *et al.* reported that during the reaction, hCNCs donated electrons to oxygen-deficient In_2O_3 to promote oxygen-vacancy formation and withdrew electrons from oxygen-

Open Access Article. Published on 10 2026. Downloaded on 17.05.26 9:18:50.
This article is licensed under a Creative Commons Attribution-NonCommercial 3.0 Unported Licence.

rich In_2O_{3-x} to prevent over-reduction to metallic In, thereby dynamically balancing the catalytic activity and structural stability (Fig. 5d).[72]

(2) Enhance the photo-induced heat effect

As functional phases, carbon materials increase the catalyst surface temperature through photo-to-thermal conversion, thereby directly driving or facilitating CO_2 reduction reactions.[104,105] The structural features of carbon materials impart them with photothermal responsiveness, making them essential functional phases in photothermal CO_2 reduction systems.

CDs broaden the optical absorption range and efficiently convert absorbed light, particularly near-infrared, into heat through non-radiative relaxation. However, due to their small particle size, limited absorption cross-section, and competitive radiative relaxation, the temperature rise induced by CDs is typically modest (20–40 °C) (Fig. 6a).[98,106,107] In contrast, CNTs exhibit strong broadband light absorption, achieving absorption efficiencies exceeding 99% across the visible to near-infrared region spanning approximately 0 to 2500 nm. This optical characteristic makes CNTs promising photothermal components for solar-driven catalytic systems.[108] In the CoPc/CNT composite catalyst, CNTs effectively harvested and converted solar energy to provide an optimal reaction temperature (around 250 °C). Compared with pristine CoPc, the composite system fully exploited the strong light-harvesting and heat-conversion capabilities of CNTs, significantly enhancing the overall catalytic performance (Fig. 6b).[30]

Biomass-derived carbon materials have also shown stable photo-to-thermal conversion performance under realistic solar irradiation. Wang *et al.* evaluated a Bi_2MoO_6/biomass-derived carbon framework (BCF) catalyst under natural sunlight and reported that its surface temperature reached approximately 137 °C (Fig. 6c), confirming its feasibility for outdoor CO_2 conversion under practical conditions.[87]

MOF-derived metal@carbon materials confine the localized heating effect induced by carbon structures directly to the vicinity of the active sites, thereby minimizing the intrinsic energy dissipation of bulk thermal catalysis.[110] Khan *et al.* reported that a high degree of graphitization in MOF-derived Ni@C catalysts enhanced near-infrared absorption and the thermal conductivity of the carbon framework, thereby improving the photo-to-thermal conversion efficiency. The study further suggested that long-wavelength radiation rather than visible light plays a more significant role in the photo-to-thermal conversion process (Fig. 6d).[109]

It is worth noting, however, that strong light-induced heat effects do not necessarily translate into high catalytic efficiency. The optimal local temperature should match the thermodynamic and kinetic requirements of the target reaction while avoiding excessive thermal energy loss or side reactions. Therefore, the design of photothermal systems should focus not solely on maximizing heat generation but rather on achieving controllable and spatially confined heating.

3.1.3 Regulatory phase for dispersion modulation and structural stabilization. In photothermal CO_2 reduction, certain carbon materials regulate the catalyst structure by enhancing the dispersion of active species and maintaining the structural stability, and are thus recognized as regulatory phases. It is worth noting that, in most catalytic systems, carbon materials are often not confined to a single role and can simultaneously

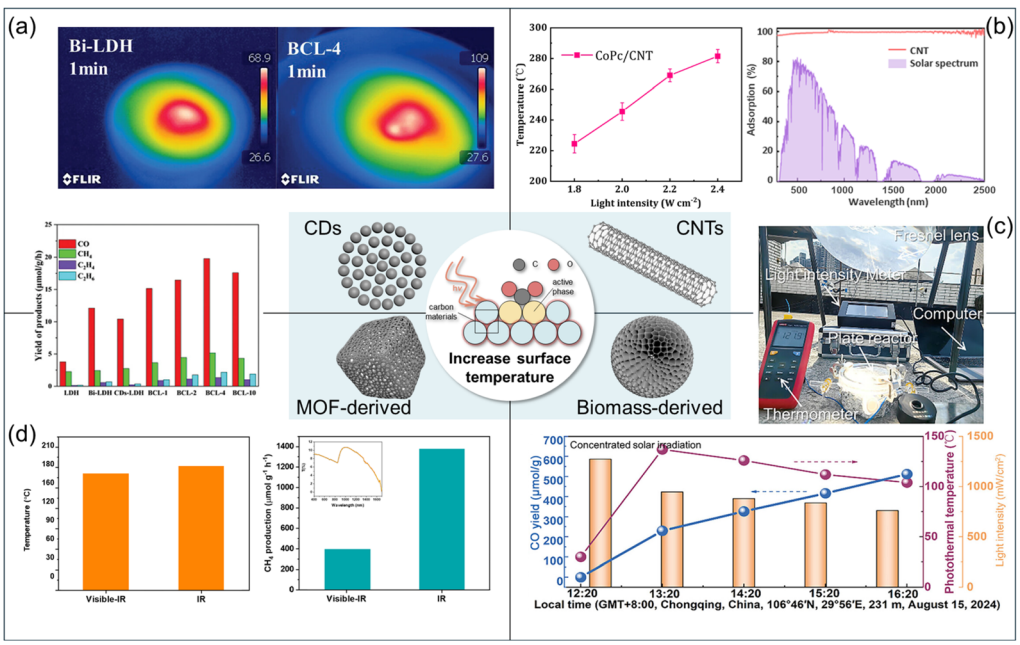

Fig. 6 Carbon-based functional phases for enhancing the photo-induced heat effect: (a) effect of CDs on surface catalytic temperature in Bi-CDs/LDH. Reproduced with permission.[98] Copyright 2024, John Wiley & Sons. (b) Effect of CNTs on surface catalytic temperature in CoPc/CNTs. Reproduced with permission.[30] Copyright 2024, John Wiley & Sons. (c) Surface catalytic temperature of Bi_2MoO_6/BCF in outdoor experiments under natural light with a condenser. Reproduced with permission.[87] Copyright 2025, John Wiley & Sons. (d) The contributions of visible and infrared light in photothermal CO_2 methanation over Ni@C. Reproduced with permission.[109] Copyright 2021, John Wiley & Sons.

 This journal is © The Royal Society of Chemistry 2026

Open Access Article. Published on 10 2026. Downloaded on 17.05.26 9:18:50.
This article is licensed under a Creative Commons Attribution-NonCommercial 3.0 Unported Licence.

function as both regulatory and functional phases. Therefore, photothermal CO_2 reduction systems using carbon materials as regulatory phases are not separately listed as a table here.

(1) Facilitating the dispersion of active phases

The ability of carbon materials to promote highly dispersed active phases primarily arises from their large surface area and abundant anchoring sites, which provide favourable conditions for the uniform distribution of catalytic components.[111] Ru nanoparticles supported on ZrO_2/C exhibit an average size of 3.2 nm, whereas those on bare ZrO_2 are around 5.5 nm, corresponding to an approximately 1.7-fold enhancement in relative dispersion induced by the presence of carbon.[68] Benefiting from both the hierarchical structure and large surface area of carbon supports, Ru nanoparticles with an average size of 1.2 nm are uniformly dispersed at high metal loadings through a simple impregnation method, enabling efficient photothermal RWGS reactions.[35] Thermal pyrolysis of Ru precursors on the carbon support further generates catalysts with coexisting Ru single atoms and clusters, in which Ru single atoms are responsible for CO_2 hydrogenation to CO, while Ru clusters promote H_2 activation and hydrogen spillover.[112] Moreover, carbon@metal composites derived from MOFs highlight the dispersion regulation capability of carbon materials. The spatial confinement effect effectively suppresses the migration and sintering of metal species, resulting in small particle sizes and well uniform distributions.[113,114] In Co/NC catalysts derived from ZIF-67, metal species are dispersed at the atomic level, efficiently allowing each atom to be functionalized as an active phase and significantly improving the metal utilization efficiency. Building on single atom stabilization, carbon materials further enable the directional construction of dual atom catalysts with controlled metal proximity.[115,116] In Ni and Fe dual atom systems, the N-doped carbon support anchors these two metal atoms to adjacent sites, such that Fe acts as the primary CO_2 activation centre, while the optimized Ni–Fe distance allows N-bridged Ni–N–N–Fe configuration to facilitate the dissociation of COOH* and HCO_3^* intermediates.[117] Beyond inorganic metal species, carbon materials also enable the dispersion of organic molecular active phases through π–π interactions. CoPc, as an active phase for the conversion of CO_2 to methanol, exhibited improved molecular dispersion on CNTs, mainly due to non-covalent π–π interactions between CoPc and the CNT surface that enable stable molecular anchoring.[30]

(2) Maintaining the stability of active phases

As a regulatory phase, carbon materials also contribute to maintaining the stability of active phases through structural and electronic features. Their framework can physically protect metal or molecular active centres while facilitating charge redistribution at the interface to prevent oxidation or over-reduction. In Ni@C catalysts, the carbon matrix has been shown to preserve the activity of Ni nanoparticles and inhibit the oxidation by H_2O during photothermal reactions.[109] The strong electronic transport and storage properties of carbon materials also play a crucial role in maintaining active phase stability. In ZIF-derived CoO_x@C catalysts, even in the absence of direct chemical bonding, interfacial electronic interactions between the carbon shell and CoO_x species create efficient charge transportation channels. Acting as an electron acceptor, the carbon shell can rapidly extract excess electrons from CoO, thereby preventing its over-reduction to metallic Co and stabilizing the active CoO species.[110] Such electronic buffering effects endow carbon-based regulatory phases with long-term durability under photothermal conditions.[118]

Overall, the regulatory phase serves as a structural stabilizer that bridges activity and durability in photothermal CO_2 reduction. By governing the spatial dispersion, redox environment, and charge flow within catalytic systems, carbon-based regulatory phases provide a foundation for constructing catalysts with both high efficiency and long-term operational stability.

3.2 Structure-induced selective photothermal CO_2 reduction on carbon materials

In the preceding sections, the multifaceted roles of carbon materials in photothermal CO_2 reduction systems have been discussed. While these functionalities establish the foundation for efficient catalysis, the ultimate performance of selective photothermal CO_2 reduction is governed by the surface reaction pathways and the evolution of key intermediates. The structural and electronic characteristics of carbon materials profoundly influence the adsorption/desorption energies and transformation dynamics of these intermediates.

3.2.1 Identification of key intermediates in CO_2 reduction. Fig. 7 outlines the representative reaction pathways for photothermal CO_2 reduction to C_1 and C_2 products over carbon materials. Generally, the conversion of CO_2 to C_1 products follows two principal routes: the COOH* pathway and HCOO* pathway. In the COOH* pathway, adsorbed CO_2^* is first hydrogenated to form COOH*, which subsequently transforms into CO*. This route is widely regarded as the primary mechanism for CO formation.[119,120] CO* is considered a key intermediate in CO_2 conversion to C_1 products, as its adsorption strength on the catalyst surface largely determines the product selectivity. Weak CO* adsorption facilitates its desorption from the surface, promoting CO formation, whereas strong adsorption favours further hydrogenation toward methane or methanol. In recent years, an alternative HCOO*-mediated pathway has also been proposed for CO formation. Although this mechanism involves the combination of unlinked hydrogen and oxygen atoms on the carbon centre of the adsorbed CO_2^*, leading to a relatively high energy barrier, surface structures and charge transfer behaviours effectively lower this barrier, making the pathway competitive under certain conditions.[90,121]

In addition, the formation of intermediates such as COH* and CHO* is regarded as a crucial branching point that determines the final product type. Further hydrogenation of COH* is considered to promote CH_4 formation, while the hydrogenation of CHO* is generally associated with CH_3OH production. Typically, COH* originates from the sequential hydrogenation process from COOH*,[122] whereas CHO* is commonly formed through the HCOO* pathway.[69] Therefore, the formation and transformation of CO*, COH*, and CHO* together constitute the key reaction network for the conversion of CO_2 to C_1 products. Modulating their adsorption strengths and reaction

Open Access Article. Published on 10 2026. Downloaded on 17.05.26 9:18:50.
This article is licensed under a Creative Commons Attribution-NonCommercial 3.0 Unported Licence.

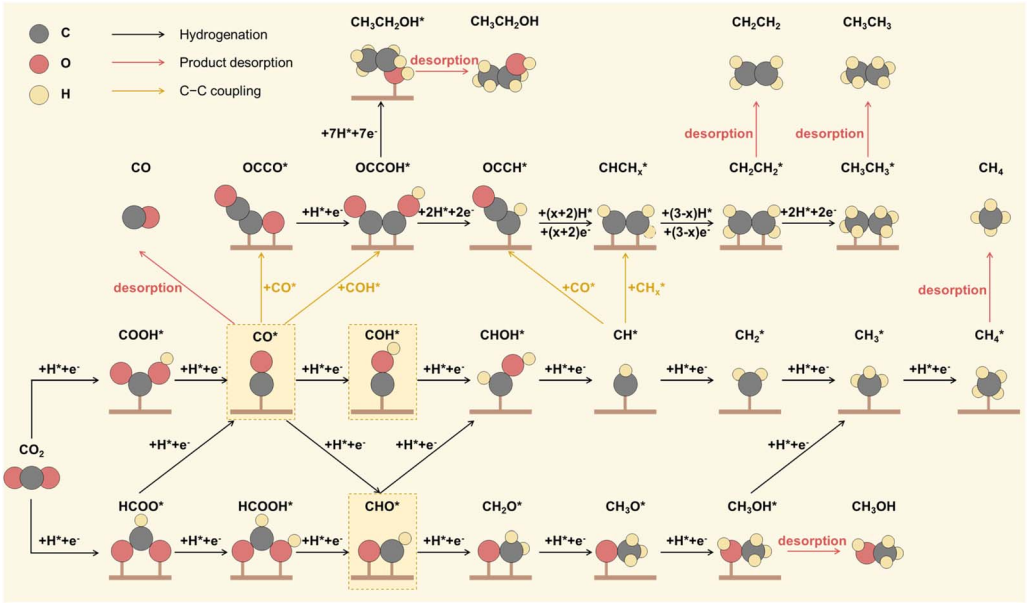

Fig. 7 Reported photothermal catalytic CO_2 to C_1 and C_2 product conversion pathways on carbon materials.

barriers is considered a central strategy for achieving selective product formation.

Due to the complex multi-electron/proton transfer processes and sluggish C–C coupling kinetics, the photothermal conversion of CO_2 to C_{2+} products over carbon materials remains highly challenging. Reported mechanisms generally proceed through two sequential steps. It involves the initial formation of C_1^* intermediates *via* the COOH* or HCOO* pathway, followed by C–C coupling between CO*, CH_x^*, or their further hydrogenation species to generate longer-chain products.[123,124] A high surface concentration of carbon-containing intermediates is recognized as a prerequisite for promoting C–C coupling, though the mechanisms governing their formation and stabilization are not yet fully understood.

3.2.2 Regulation of key intermediate adsorption behaviours in photothermal CO_2 reduction through incorporation of carbon materials. The incorporation of carbon materials has been shown to effectively modulate CO* desorption, thereby altering the reaction pathway and product distribution. For example, Ma *et al.* synthesized a Co@NC photothermal catalyst and found that the surface carbon layer significantly reduced the CO* adsorption energy. This promoted CO desorption and enhanced both the yield and selectivity toward CO.[90] Similarly, Guo *et al.* reported that the introduction of reduced GO into Bi_2MoO_6–I quantum dots decreased the CO* desorption energy from 4.27 eV to 0.48 eV, thereby accelerating the forward CO_2 reduction process.[86]

In some studies, the emergence of COH* or CHO* intermediates has been viewed as a descriptor for product selectivity. Ren *et al.* investigated the free energy of CO* hydrogenation to predict the product selectivity of photothermal CO_2 reduction and found that the activation barrier for the methanol pathway (CO* to CHO*) was much lower than that for the CO (CO* to CO) or CH_4 (CO* to COH*) routes, suggesting a kinetic preference for methanol formation. Experimental results further confirmed this prediction, with CoPc/CNT achieving a methanol selectivity of 99% and a yield of 2.4 mmol g_{cat}^{-1} h^{-1} under a moderate light intensity of 2.0 W cm^{-2}.[30]

Although studies on the conversion of CO_2 to C_{2+} products over carbon-based catalysts remain limited, recent findings suggested that carbon structures can significantly promote selective C–C coupling. Wang *et al.* demonstrated that in TiO_2@NC nanospheres, interfacial charge redistribution between TiO_2 and NC led to electron transfer from TiO_2 to the NC microchannels, where electrons accumulated and enhanced the probability of C–C coupling.[125] Another work has shown that in Co/NC catalysts, an increased ratio of graphitic nitrogen species improved the basicity of the surface, strengthened CO_2 adsorption, and increased the concentration of surface carbon intermediates, leading to the formation of C_{2+} products.[124]

In summary, carbon materials enable selective CO_2 conversion by regulating the adsorption and transformation of key intermediates such as CO*, COH*, and CHO*. Future studies that integrate *in situ* spectroscopic characterization with theoretical simulations to track the dynamic evolution of intermediates are expected to provide fundamental guidance for achieving control and high selectivity in photothermal CO_2 reduction.

4 Rational modification strategies of carbon materials for photothermal CO_2 reduction

The functions that originated from native properties of carbon materials alone are sometimes insufficient for high-efficiency CO_2 conversion. Thus, targeted modification strategies further

 This journal is © The Royal Society of Chemistry 2026

Open Access Article. Published on 10 2026. Downloaded on 17.05.26 9:18:50.
This article is licensed under a Creative Commons Attribution-NonCommercial 3.0 Unported Licence.

strengthening or refining these functions are introduced in this section. In addition, data-oriented AI-assisted catalyst design has emerged as a promising tool to accelerate material optimization of carbon-based photothermal systems.

4.1 Heteroatom doping for tailoring surface chemistry

Heteroatom doping is a modification strategy that introduces non-metallic atoms such as N, B, P, and S into carbon materials to regulate their catalytic activity.[126,127] This approach allows tuning of the electronic distribution and local chemical environment, thereby improving the reactant adsorption capability, adjusting the adsorption energy of intermediates, and optimizing the distribution of active sites. In current studies on photothermal CO_2 reduction over carbon materials, most reported doping systems have focused on N doping.

When carbon materials serve as active phases, N doping supplements their intrinsic physical CO_2 adsorption sites with additional chemical adsorption sites, thereby allowing more CO_2 molecules to participate in the reaction. This enhancement has been confirmed in photothermal CO_2 reduction systems producing CO, CH_4, and C_2H_6.[124] Xia *et al.* proposed that introducing N atoms into the carbon lattice of graphene significantly altered the electronic distribution of the carbon surface, thereby increasing its surface polarity (Fig. 8a).[128] The enhanced polarity generated localized regions of positive and negative charges, which interacted electrostatically with the quadrupolar charge distribution of CO_2, thereby strengthening chemical adsorption.[129,130] Further studies by Ma *et al.* showed that pyridinic-N, possessing lone-pair electrons, provided Lewis basic sites that interacted with the Lewis acidic CO_2, increasing the adsorption affinity and inducing molecular bending.[131]

In addition, during the conversion of CO_2 to CO, N doping has been reported to promote the desorption of the key intermediate CO*, thereby increasing the yield and selectivity toward CO. Ning *et al.* found that in Co@CoN&C catalysts, N incorporation formed stable Co–N coordination structures that enable electron transfer from Co to N, lowering the electron density around the metal centre (Fig. 8b). This adjustment weakened excessive hydrogenation activity and promoted the formation of HCOO* and the desorption of CO*, leading to improved CO selectivity.[27] Similarly, it has been reported that the Ru–N_4 coordination structure in Ru/hNCNC catalysts reduced the CO adsorption energy, thus facilitating CO_2 conversion to CO with high selectivity (Fig. 8c).[112]

Furthermore, heteroatom doping has also been reported to facilitate the dispersion of active sites. As discussed earlier, N atoms, possessing lone-pair electrons, can create localized regions with uneven electron density on the surface of carbon materials. These regions can also interact with metal precursors through electrostatic attraction or chemical coordination, resulting in improved metal dispersion and suppression of aggregation during high-temperature treatments.[132] Chen *et al.* compared Ru/hCNC and Ru/hNCNC catalysts and observed

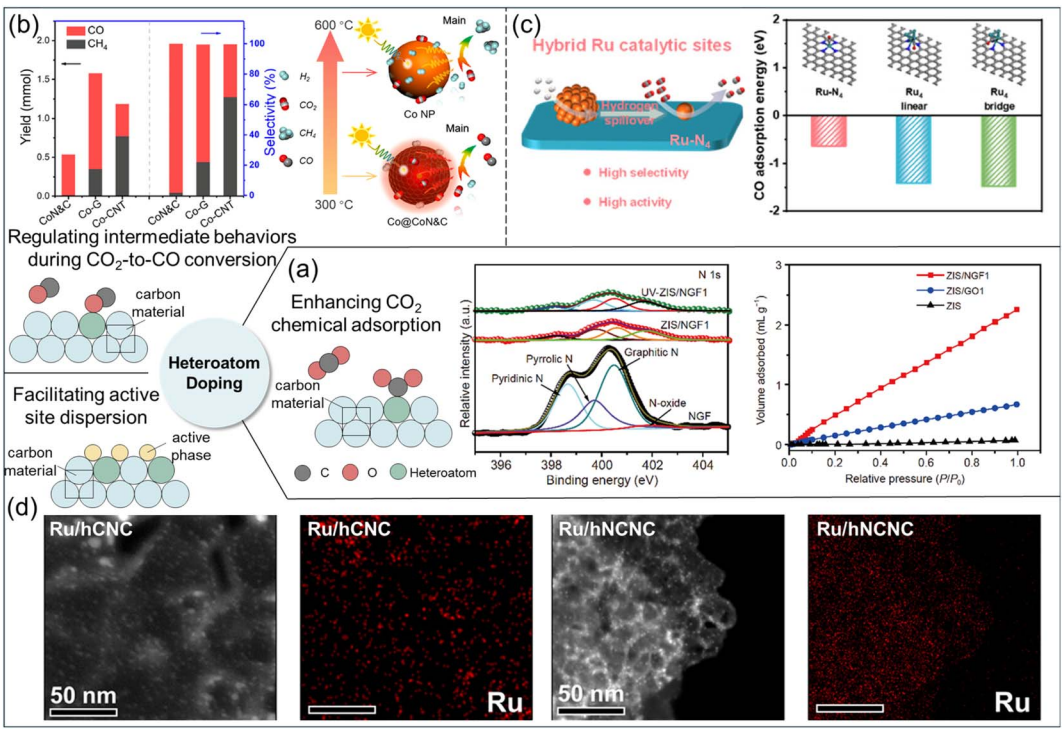

Fig. 8 Heteroatom doping in photothermal CO_2 reduction over carbon materials. (a) Heteroatom doping for enhancing CO_2 chemical adsorption. Reproduced with permission.[128] Copyright 2020, Science China Press and Springer-Verlag GmbH, Germany. Heteroatom doping for regulating intermediate behaviours during the conversion from CO_2 to CO over (b) Co@CoN&C and (c) Ru/hNCNC. Reproduced with permission.[27] Copyright 2020 American Chemical Society. Reproduced with permission.[112] Copyright 2025, John Wiley & Sons. (d) Heteroatom doping for facilitating active site dispersion. Reproduced with permission.[35] Copyright 2024, American Chemical Society.

Open Access Article. Published on 10 2026. Downloaded on 17.05.26 9:18:50.
This article is licensed under a Creative Commons Attribution-NonCommercial 3.0 Unported Licence.

that N doping promoted the formation of ultrasmall Ru nanoparticles (Fig. 8d), which was attributed to the strong interaction between pyridinic N lone-pair electrons and Ru^{3+} ions.[35]

Although current research on heteroatom-doped carbon-based catalysts for photothermal CO_2 reduction mainly focused on N, other non-metallic elements also show promising potential. Wang *et al.* reported that B doping in a photothermal CO_2 cycloaddition system introduced abundant Lewis acidic sites in the hollow mesoporous carbon, which strongly interacted with oxygen atoms in CO_2 molecules. The electron-deficient nature of B further promoted directional charge transfer, accelerating the coupling between CO_2 and epoxides.[133]

4.2 Interface engineering for promoting carrier dynamics

Carbon materials possess tunable electronic structures, enabling them to be incorporated into interface engineering frameworks to enhance charge separation and directional carrier migration. By facilitating more efficient redistribution of photogenerated carriers, these interfaces strengthen the redox capability required for CO_2 conversion.[134,135]

Carbon materials such as graphene and highly graphitized porous carbons exhibit semi-metallic electronic behaviour, allowing them to act as the metallic component in Schottky junctions formed with semiconductors.[136,137] In the ZnO/graphene system, photogenerated electrons in ZnO can transfer to graphene, while holes remained in ZnO by Schottky barrier, suppressing recombination.[138] Similarly, in the graphitic carbon nitride (NCN-T)/Cu@C system, the Fermi level difference drove electron migration from NCN-T to Cu@C, and the resulting Schottky barrier prevented the electron backflow, thereby promoting directional charge separation and forming a local electron-rich region for CO_2 reduction (Fig. 9a).[139]

Owing to their tunable electronic structures, carbon materials can achieve band alignment with various semiconductors to form heterojunctions. Type-II and S-scheme heterojunctions are among the most commonly reported configurations in carbon-based photothermal CO_2 reduction systems. In Type-II heterojunctions, the staggered band alignment enables physical separation of photogenerated carriers. As exemplified by the Fe@C/Ni_2P heterojunction system, electrons spontaneously migrated to Fe@C, while holes accumulated in Ni_2P, resulting in spatially separated charge carriers (Fig. 9b).[89] S-scheme heterojunctions can induce spontaneous electron transfer by Fermi-level differences and generate an internal electric field, which directs charge separation while allowing low-energy carriers to re-combine at the interface and retaining high-energy carriers with stronger redox capability.[140] In the

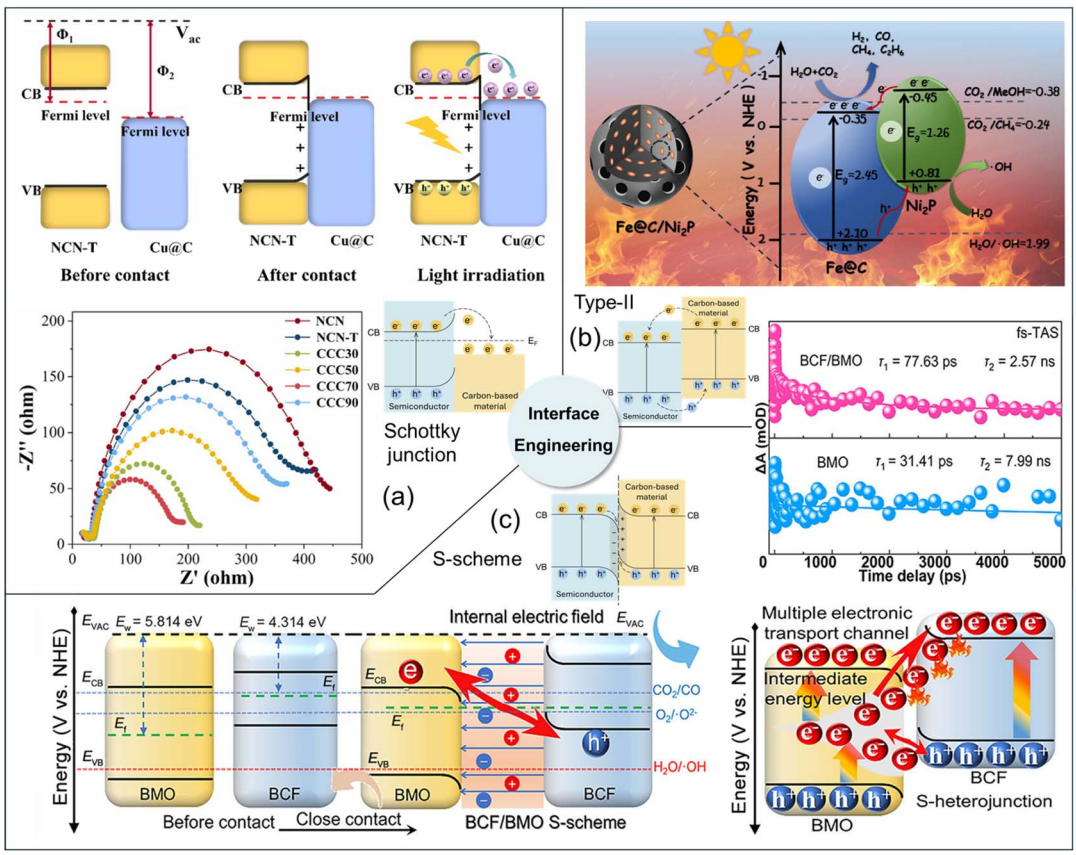

Fig. 9 Interface engineering for improved charge separation and directional carrier migration in photothermal CO_2 reduction over carbon materials: (a) the Schottky junction between Cu@C and NCN-T. Reproduced with permission.[139] Copyright 2024, Elsevier. (b) Type-II heterojunction Fe@C and Ni_2P. Reproduced with permission.[89] Copyright 2024, Elsevier. (c) The S-scheme heterojunction between Bi_2MoO_6 and BCF. Reproduced with permission.[87] Copyright 2025, John Wiley & Sons.

 This journal is © The Royal Society of Chemistry 2026

Open Access Article. Published on 10 2026. Downloaded on 17.05.26 9:18:50.
This article is licensed under a Creative Commons Attribution-NonCommercial 3.0 Unported Licence.

NiO@Ni/N-doped carbon (NC) system, electrons transferred from NiO@Ni to NC to establish an internal electric field that drove directional carrier migration under illumination, enabling the preservation of strongly reducing electrons in NiO@Ni and strongly oxidizing holes in NC for CO_2 conversion.[141] In addition, introducing an interfacial electron bridge can further enhance cross-interface charge transfer,[85] as demonstrated in the Bi_2MoO_6/BCF system, where the N–C–O–Bi covalent bond reduced the interfacial distance and lowered the electron transfer barrier (Fig. 9c).[87]

Moreover, Z-scheme heterojunctions represent an emerging interfacial engineering strategy for photothermal CO_2 reduction, which can enhance interfacial-electron-induced CO_2 activation.[142–144] Future studies should focus on elucidating how effective charge separation and directional carrier transport promote CO_2 activation and govern product selectivity, thereby supporting the development of controlled and selective CO_2 conversion.

4.3 Morphological and structural design for light-induced thermal field management

Morphology and structural design further enabled light-heat regulation on broadband-absorbing carbon materials, thereby generating suitable photo-induced thermal effects for CO_2 reduction.[145] One primary purpose of morphological and structural engineering was to enhance the capture and utilization of incident light. Han *et al.* designed a frame-in-cage dodecahedral hybrid featuring hierarchical porous channels that promoted multiple internal reflections and scattering, which increased the light absorption efficiency (Fig. 10a).[146] A lotus-pod-like hierarchical porous carbon structure was reported to effectively trap and scatter photons, greatly improving the photo-to-thermal conversion efficiency, while its graphitized framework with high thermal conductivity allowed rapid heat accumulation (Fig. 10b). Under an illumination intensity of 2.8 W cm^{-2}, the catalyst surface temperature reached approximately 440 °C within 20 seconds.[28]

Beyond enhancing light absorption and heat accumulation, localized heating at active sites also represented a key strategy for improving photo-induced thermal effects. Wang *et al.* demonstrated that the intimate interfacial contact between Co and the carbon framework enabled efficient heat transfer to Co active sites, resulting in rapid temperature rise at reaction centres (Fig. 10c).[28] The interfacial contact configuration further governed the degree of local heating. Compared with the planar-contact carbon black (CB)/Cu/ZnO/Al_2O_3 (CZA) catalyst, the interwoven-contact oxidized carbon black (oCB)/CZA system maintained a similar overall temperature under identical

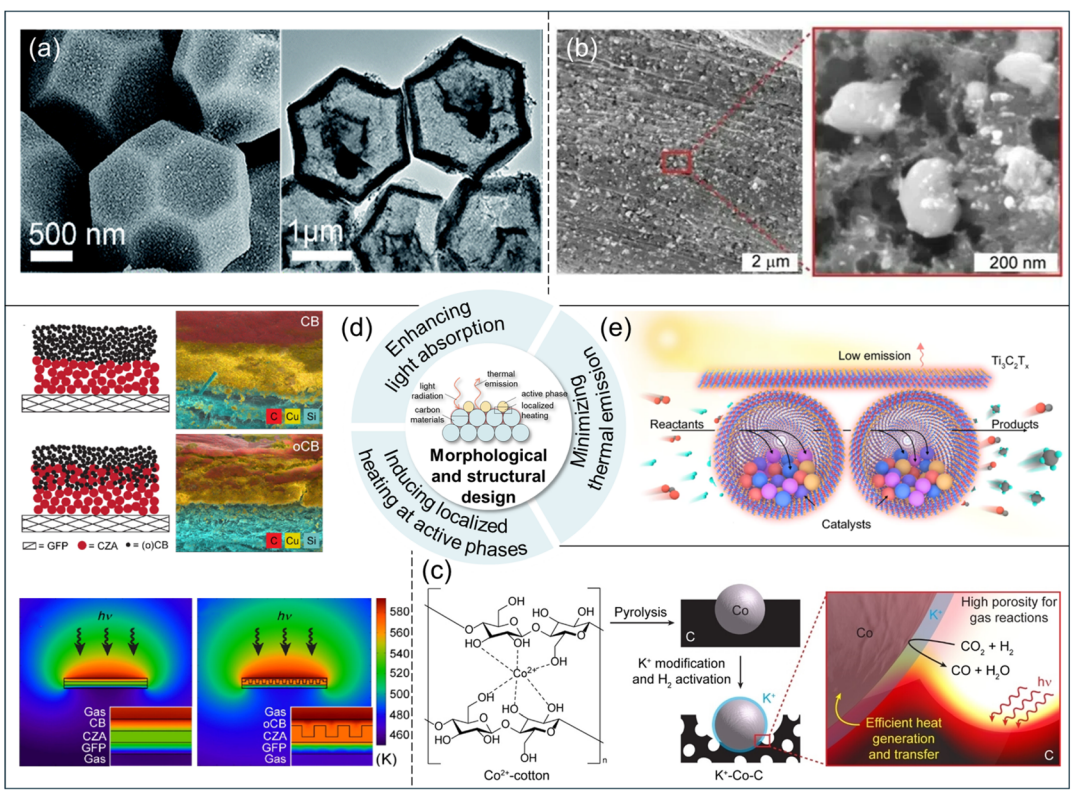

Fig. 10 Morphological and structural design for photo-to-thermal conversion in CO_2 reduction over carbon materials: morphological and structural design to enhance light adsorption over (a) ZnSe–CdSe@NC FC and (b) K^+–Co–C. Reproduced with permission.[146] Copyright 2022, The Royal Society of Chemistry. Reproduced with permission.[28] Copyright 2023, John Wiley & Sons. Morphological and structural design to induce localized heating in active phases over (c) K^+–Co–C and (d) CB/CZA and oCB/CZA. Reproduced with permission.[28] Copyright 2023, John Wiley & Sons. Reproduced with permission.[37] Copyright 2025, The Author(s). (e) Morphological and structural design to minimize thermal emission. Reprinted with permission.[149] Copyright 2024 Springer Nature.

Open Access Article. Published on 10 2026. Downloaded on 17.05.26 9:18:50.
This article is licensed under a Creative Commons Attribution-NonCommercial 3.0 Unported Licence.

illumination but achieved high local temperatures at active sites, increasing the methanol production rate from 2.93 to 4.91 mmol g_{CZA}^{-1} h^{-1} (Fig. 10d).[37]

Moreover, morphological and structural design has also been reported to minimize thermal emission, thereby further improving the photo-to-thermal efficiency. Yang *et al.* reported a Janus-type Ru@m-$Ti_3C_2T_x$ catalyst featuring one smooth and one porous surface. The smooth side exhibited a very low mid-infrared emissivity of about 21%, enabling local heat confinement, while the porous side facilitated efficient mass transfer of reactants and products, resulting in enhanced CH_4 production (Fig. 10e).[147] This morphology-controlled approach to suppress thermal radiation losses can also be extended to carbon-based catalytic systems. By rationally designing structural heterogeneity within carbon materials, it is possible to achieve high light absorption while minimizing thermal dissipation, thereby enabling efficient and precise photo-induced heat management.

4.4 AI-empowered smart design of carbon-based photothermal catalysts

While the above modification strategies primarily rely on experimental tuning, the large number of compositional, structural, and operational variables make traditional trial-and-error approaches insufficient for efficiently identifying optimal catalyst configurations. Thus, data-driven AI methods offer a complementary pathway to accelerate catalyst discovery and guide the rational optimization of carbon-based photothermal systems. AI integrates advanced concepts from computer science, mathematics, and statistics to enable computational systems to emulate human reasoning, inference, and decision-making to a certain extent.[148] As one of the core methodologies of AI, machine learning (ML) is designed to extract the underlying patterns from large datasets through algorithmic modelling and to apply these patterns to predict or classify new data.[150] In practical applications, ML models can capture complex nonlinear correlations between input variables and output responses, providing a robust analytical tool for the design and optimization of carbon-based photothermal catalysts for CO_2 reduction. The development of an ML model typically involves five steps: problem identification, dataset construction, model training, model evaluation, and model deployment.[151] Finally, evaluation metrics such as absolute error, coefficient of determination, mean absolute error, and mean squared error are employed to assess the generalization ability of the model or to compare the performance of different AI models.[152]

The physicochemical properties and catalytic performance of carbon materials are jointly determined by synthesis conditions, including feedstock composition and processing parameters.[153] In the case of biochar synthesis, the composition of biomass feedstock and key pyrolysis parameters, such as temperature and residence time, have been widely investigated for their influence on product yield and properties. Recent studies have focused on applying AI to predict the biochar yield and CO_2 adsorption performance[154,155] while also emphasizing that ML approaches, including artificial neural networks (ANN), hold great promise for guiding future biochar production.[156,157] Manatura *et al.* conducted a comprehensive review of biomass pyrolysis and highlighted the critical role of ANN models in process optimization. However, they also noted that the limited understanding of the internal mechanisms of AI algorithms, often described as black box systems, highlights the need to integrate computational results with thermodynamic and kinetic experimental data for better interpretability.[158] Li *et al.* introduced explainable ML techniques, such as feature importance ranking and SHAP analysis, to identify the dominant structural and chemical features governing CO_2 adsorption performance, including the pore size distribution and surface functional groups.[159] Building on these findings, they further applied active learning and particle swarm optimization algorithms to iteratively determine the optimal synthesis parameters, thereby improving the adsorption properties of biochar.[160,161] Together, these studies demonstrate the potential of AI-assisted methodologies to accelerate the rational design and controlled synthesis of carbon-based photothermal catalysts.

5 Environmental and economic benefits of carbon-driven photothermal CO_2 reductions

Translating the laboratory-scale advances in carbon-based photothermal CO_2 reduction into practical and sustainable systems requires a multidimensional evaluation framework that extends beyond catalytic performance alone. The economic feasibility and environmental sustainability of these catalysts have become equally important for assessing their real-world applicability and scalability. The integration of TEA and LCA offers a comprehensive platform for the systematic evaluation of carbon-based photothermal CO_2 catalysts.

5.1 Techno-economic analysis

TEA serves as a systematic framework for evaluating the overall performance of a process, product, or service in terms of both technical feasibility and economic viability. As an interdisciplinary approach, TEA typically integrates key steps such as process modelling, engineering design, and economic assessment. Its primary objective is to quantitatively analyze factors such as cost, revenue, risk, and uncertainty, thereby elucidating the input–output relationships and potential economic competitiveness of a technology over its full life cycle.[162] Introducing TEA into the field of photothermal CO_2 reduction not only provides a quantitative analytical tool for catalyst design and process optimization but also establishes an economic foundation for the sustainable and scalable deployment of photothermal conversion technologies.[163]

Compared with conventional metal oxide supports, carbon materials exhibit economic advantages. For instance, as one of the most widely used inorganic supports, the market price of P25 TiO_2 produced by Evonik ranged between USD 50 000 and 100 000 per t.[164] In contrast, commercial powdered activated

 This journal is © The Royal Society of Chemistry 2026

Open Access Article. Published on 10 2026. Downloaded on 17.05.26 9:18:50.
This article is licensed under a Creative Commons Attribution-NonCommercial 3.0 Unported Licence.

carbon costs only USD 1100–1700 per t and, after appropriate surface modification, provides a high surface area and abundant pore volume, making it an efficient yet low-cost catalyst support. Moreover, biomass-derived carbon materials demonstrate even stronger economic competitiveness owing to their renewable feedstock sources and recyclability. Biochar derived from waste tires has an estimated production cost of merely USD 299 per t.[165] Globally, the biochar market has experienced rapid expansion, reaching USD 1.85 billion in 2021 and projected to grow to USD 3.99 billion by 2026, surpassing USD 6.3 billion by 2031.[166] This rapid market growth highlights the significant potential of carbon materials in renewable energy and carbon cycle applications, further confirming their economic advantage and industrial scalability in photothermal CO_2 reduction.

Extensive studies have demonstrated that carbon materials, particularly biomass-derived carbon materials, can be produced within an economically acceptable cost range. Haeldermans *et al.* conducted a large-scale techno-economic analysis of biochar production from various waste feedstocks through conventional pyrolysis processes. Their results indicated that when the minimum selling price of biochar ranged between €436 and €863 t^{-1}, the production facilities remained economically viable.[167] Nematian *et al.* analysed the cost structure of biochar production from orchard biomass using a portable pyrolysis system and reported that the production cost ranged from USD 448.78 to 1846.96 per t, with a 90% confidence interval between USD 571 and 1455 per t.[168] Thus, biochar derived from diverse waste sources can be produced at a manageable and competitive cost, further validating its potential as a sustainable and low-cost carbon material for scalable catalytic applications.

Although the cost of biochar is primarily determined by its feedstock, further processing to obtain high-performance carbon materials can substantially increase the overall product price. Excessive pretreatment of raw materials or the use of costly post-processing procedures to meet the desired material quality requirements often becomes a major contributor to production costs. Zbair *et al.* produced a high-performance adsorbent through microwave-assisted pyrolysis and chemical activation of apricot shells. The estimated cost for this laboratory-scale process reached approximately USD 27 800 per t, with chemical activation reagents accounting for the largest portion of the total production cost.[169] Chakraborty *et al.* estimated the production costs of wood biochar and steam-activated wood biochar to be USD 3587 and 3737 per t, respectively.[170] Nevertheless, these costs are expected to decrease significantly under large-scale industrial production. It is therefore essential to establish a balance between the processing cost and optimal catalytic performance. The fabrication of carbon-based photothermal catalysts should adhere to a cost-minimization principle. For example, the transportation of feedstocks may constitute a substantial portion of the overall material cost; thus, matching the production facilities geographically with local raw material sources can effectively reduce the logistics and storage expenses.[171] Moreover, process integration, such as utilizing by-products or intermediates generated during carbon production, offers a promising route to further lower the overall operational expenditure.[172] When carbon materials are used as catalyst supports, the optimization strategy should also focus on reducing the amount of noble metals or metal oxides required while carefully balancing the processing cost against catalytic performance to achieve an economically optimized design.

Numerous studies have identified biochar as a promising low-cost gas adsorbent,[173] but its economic advantage as a catalyst support remains insufficiently demonstrated. In addition, the reusability and end-of-life (EoL) treatment of carbon-based catalysts also play a critical role in determining their overall economic performance. Therefore, future TEA of carbon-based photothermal catalysts should systematically incorporate these factors to ensure realistic and scalable economic evaluations.[174,175]

5.2 Life-cycle assessment

LCA is a standardized methodology for qualitatively and quantitatively evaluating the environmental impacts associated with a product throughout its entire life cycle. By analysing resource and energy inputs, pollutant emissions, and waste generation at each stage, LCA provides a comprehensive framework to assess the overall environmental performance of a process or material.[176,177] The primary goal of LCA studies is to identify environmental hotspots and propose strategies for process optimization. The typical procedure involves three key stages: defining the system boundary (Life Cycle Inventory, LCI), analysing the established system (Life Cycle Inventory Analysis, LCIA), and conducting the final sustainability evaluation (Life Cycle Costing, LCC).[178,179] Among these, the construction of the LCI plays a pivotal role in determining whether a production stage ("cradle-to-gate") or the entire production chain ("cradle-to-grave") is considered sustainable. Together, these steps form the analytical foundation of LCA and provide a framework for the environmental assessment of carbon materials (Fig. 11).

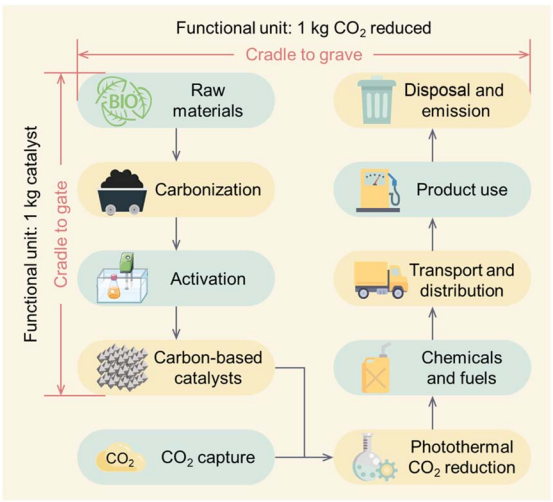

Fig. 11 General system boundary for carbon-based photothermal CO_2 reduction.

Open Access Article. Published on 10 2026. Downloaded on 17.05.26 9:18:50.
This article is licensed under a Creative Commons Attribution-NonCommercial 3.0 Unported Licence.

The pyrolysis-based synthesis of photothermal carbon materials has received increasing attention in LCA research due to significant energy demand and potential pollutant emissions. Among various impact indicators, the global warming potential (GWP) is the most widely used metric, as it directly reflects the degree of climate impact or the mitigation achieved through process improvement. Generally, the use of chemical reagents, such as acids, bases, or other activating agents, during carbon-based material preparation contributes substantially to GWP, while energy consumption and related emissions are additional major contributors. Thus, adopting low-emission energy sources (*e.g.*, renewable electricity, solar, or biomass-derived heat) and optimizing chemical treatment steps can significantly reduce the environmental footprint of carbon-based material synthesis.[180] Dutta and Raghavan conducted an LCA of biochar production using agricultural and forestry residues as feedstocks and found that pyrolysis-based production offered superior carbon sequestration compared with direct biomass combustion.[181] Barrola *et al.* compared different thermochemical conversion routes and demonstrated that slow pyrolysis provided the highest carbon reduction efficiency, offsetting 0.07–1.25 tons of CO_2 equivalent per ton of feedstock.[182] These studies collectively indicate that the environmental impacts of carbon-based material production are primarily influenced by feedstock selection and process optimization.

For application-oriented studies, the first LCA integrating biochar catalysts was reported by Chun Minh Loy *et al.* In their work, wheat straw-derived activated carbon was evaluated using a gate-to-gate approach and the Impact 2002+ method, which considers four categories: resource consumption, climate change, human health, and ecosystem quality. The results revealed that the separation step during catalyst preparation contributed most significantly to the impacts on human health and climate change, emphasizing the importance of improving separation processes and conducting further LCAs of metal-loaded biochar catalysts.[183] In a subsequent study, Cao *et al.* performed a cradle-to-gate LCA comparing catalysts derived from different biomass types, including seaweed, microalgae, and lignocellulosic biomass, and found that lignocellulosic-derived catalysts exhibited the lowest GWP, only 0.83 kg CO_2 equivalent per kilogram of catalyst, demonstrating superior environmental sustainability.[184]

Beyond production, EoL management is another crucial aspect of the life cycle that determines the overall sustainability of carbon-based catalytic systems. Common EoL strategies include regeneration, incineration, and landfilling. The inherent physical adsorption characteristics and catalytic activity of carbon-based catalysts generally ensure good regeneration performance. For example, hydrochar-supported Ni catalysts showed performance decay over five consecutive cycles, while an *in situ* N_2 regeneration treatment effectively reactivated the catalyst by suppressing sintering and enabling redispersion.[185] Regeneration can extend the catalyst lifespan and reduce waste emissions, though performance degradation may occur after multiple cycles. Incineration allows partial energy recovery, substituting fossil fuels, but may lead to pollutant formation; valuable metals should be recovered during this process. Landfilling requires ensuring permanent immobilization of contaminants to prevent leaching or secondary pollution. Kozyatnyk *et al.* conducted a cradle-to-grave LCA of carbon materials and demonstrated that regeneration led to the lowest environmental impact, followed by landfilling, whereas incineration without energy recovery imposed the highest environmental burden.[186] Consequently, integrating regeneration strategies and process coupling into the catalyst design phase can maximize both the environmental and economic sustainability of carbon-based photothermal CO_2 reduction systems.

At the current stage of research, TEA and LCA are often limited by uncertainties arising from data acquisition, process modelling, and parameter estimation. Conventional approaches address these uncertainties through sensitivity and uncertainty analyses to identify the factors that most strongly influence the results.[179] However, as the amount and complexity of experimental and modelling data continue to increase, these traditional methods become insufficient for capturing the nonlinear and multidimensional relationships among variables. The integration of ML with TEA and LCA frameworks provides an opportunity to overcome these limitations by enabling data-driven modelling and pattern recognition, thereby improving the predictive accuracy and allowing the

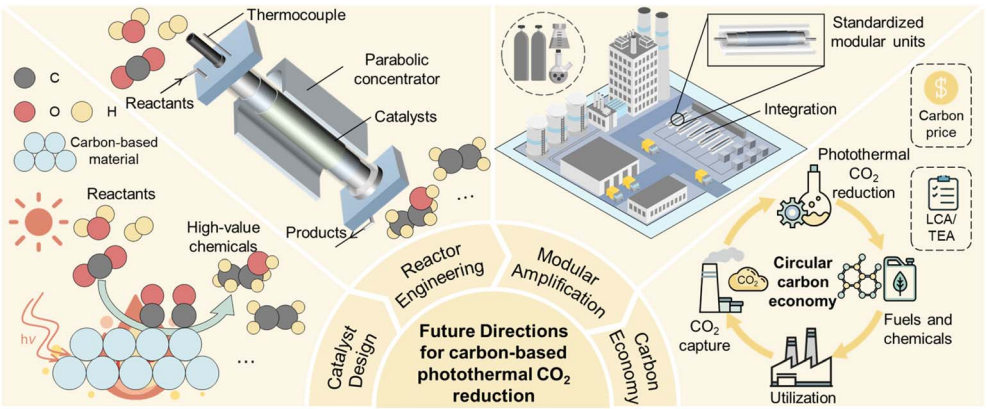

Fig. 12 Future directions of carbon-based photothermal CO_2 reduction.

 This journal is © The Royal Society of Chemistry 2026

Open Access Article. Published on 10 2026. Downloaded on 17.05.26 9:18:50.
This article is licensed under a Creative Commons Attribution-NonCommercial 3.0 Unported Licence.

derivation of more generalizable conclusions. Cheng *et al.* applied ML models to predict the properties of hydrothermally treated lignocellulosic biochar, as well as the energy investment return ratio and global warming potential of the resulting products.[187] In subsequent studies, they incorporated the influence of different biomass precursors into their analysis to predict the market selling price of biochar, providing a foundation for its large-scale production.[188]

Such methodologies can be extended to the research and evaluation of carbon-based photothermal catalysts. By coupling ML with TEA/LCA frameworks, it is possible to achieve efficient prediction and optimization not only from the perspective of photothermal performance but also in terms of cost and life cycle impacts. For example, the construction of various carbon-based composite systems can simultaneously influence the catalytic activity, material cost, energy consumption, and recyclability. Likewise, synthesis methods such as chemical vapor deposition, solvothermal processing, or templating exhibit distinct differences in energy requirements and environmental footprints. ML-driven TEA/LCA models can integrate these parameters for coordinated analysis, enabling the establishment of quantitative correlations among performance, cost, and environmental benefits. This integrated approach provides a data-informed and systematic foundation for the sustainable design, optimization, and industrial implementation of carbon-based photothermal catalysts for CO_2 reduction.

6 Conclusions and future prospects

Carbon materials provide a platform for constructing efficient photothermal CO_2 reduction systems by integrating photogenerated, thermo-driving forces and their synergistic effects. Their intrinsic structural and electronic features enable multifunctional roles in CO_2 adsorption, carrier transportation, heat conversion, structural regulation, and product selectivity. Advances in modification strategies, including heteroatom doping, interface engineering, and morphological or structural design, have demonstrated effective routes to overcome current limitations, particularly when combined with AI-assisted optimization strategies that accelerate catalyst screening and guide rational material development. Beyond catalyst engineering, a comprehensive understanding of the environmental and economic implications through LCA and TEA is essential for providing detailed information of photothermal CO_2 conversion. Continued progress requires the contributions of material innovation, reactor-level control, system-level design, policy and sustainability frameworks (Fig. 12). These coordinated efforts will facilitate the transition of carbon-based photothermal technologies toward practical CO_2 utilization, supporting long-term climate mitigation and contributing to the development of a circular carbon economy.

Currently, most carbon-based photothermal CO_2 reduction systems predominantly yield CO or CH_4, whereas the production of C_{2+} chemicals such as ethylene and ethanol aligns more closely with the goal of CO_2 valorisation. The principal challenge arises from the inherently sluggish kinetics associated with C–C coupling. Thus, advancing toward C_{2+} products require finely tuned structural modulation of carbon-based catalysts. Modification strategies directed toward stabilizing C_1 intermediates and promoting their effective coupling, including functional-group regulation within carbon frameworks, incorporation of alloy sites, and construction of charge-polarized dual-active centres, should be further developed. The integration of advanced *in situ* spectroscopic techniques, machine-learning-assisted catalyst screening, and material-acceleration platforms is expected to accelerate the discovery of highly selective C_{2+} catalytic sites. Beyond product selectivity toward high-value C_{2+} chemicals, long-term stability is widely regarded as an equally critical design objective for carbon-based photothermal catalysts. While conventional CO_2 conversion technologies have already demonstrated continuous operation over hundreds to thousands of hours,[189,190] photothermal CO_2 reduction systems remain markedly behind in terms of durability.[191,192] Bridging this gap calls for stability-oriented catalyst design, with particular emphasis on resistance to carbon deposition, preservation of carbon framework integrity, and suppression of active-site deactivation under prolonged light irradiation and thermal cycling.

Catalyst optimization alone is insufficient, and the transport processes within the reactor must be treated as explicit design variables. Efficient photothermal CO_2 reduction therefore relies on the coordinated regulation of light distribution, thermal management, and mass transfer inside the reactor. Current systems frequently exhibit non-uniform temperature profiles, local overheating, and heat loss. Future reactor designs should therefore focus on optimizing the spatial arrangement of carbon materials, tailoring light and heat flux distributions, and developing precise temperature-monitoring technologies to achieve accurate control of photo-induced thermal fields. For systems targeting liquid products such as methanol or ethanol, rapid reactant delivery and product removal are essential, which may be facilitated by gas–liquid–solid multiphase partition flow design to improve selectivity. Finally, establishing comprehensive multi-field coupled models will enable a systematic evaluation of bed architecture, flow rates, and light-intensity distributions during the design stage, thereby supporting the translation of carbon-based photothermal CO_2 reduction from laboratory studies to engineering applications.

Future development of photothermal CO_2 reduction also requires a system-level consideration of deployment modes. Unlike conventional catalytic technologies that typically rely on centralized large-scale facilities, photothermal catalysis depends on solar irradiation and generates localized thermal fields, making it inherently suitable for distributed and modular configurations. However, current photothermal CO_2 reduction reactors remain largely limited to small batch or flow devices, with few standardized modules that can be replicated, scaled, or adapted to diverse operating conditions. Future research should therefore focus on developing standardized photothermal catalytic modules with tunable light-to-heat architectures, stable thermal management, and flexible integration interfaces. Such modular units can be scaled through parallel assembly and deployed directly at industrial CO_2 capture point sources, enabling low-cost on-site CO_2 conversion

Open Access Article. Published on 10 2026. Downloaded on 17.05.26 9:18:50.
This article is licensed under a Creative Commons Attribution-NonCommercial 3.0 Unported Licence.

and utilization. Given the strong dependence of photothermal catalysis on illumination intensity, achieving dynamic steady-state operation requires intelligent control strategies. Future developments should incorporate real-time sensing, data-driven modelling, and predictive energy management to enable adaptive regulation of light distribution, heat flux, and reactant–product transport, thereby maintaining stable operation under fluctuating solar conditions.

The long-term development of photothermal CO_2 reduction must align with broader sustainability and circular-economy objectives. Progress achieved at the catalyst, reactor, and system levels collectively provides the foundation for integrating carbon-based photothermal technologies into future carbon-management frameworks. However, further advances are required to translate these developments into sustainable practice. A key priority is the establishment of effective carbon-pricing mechanisms, as the low cost of CO_2 emissions and the limited market value of CO_2-derived products remain major constraints on modular deployment. Appropriate carbon taxes and emission-trading schemes can shift CO_2 from an emission liability to a tradable feedstock, thereby improving the economic feasibility of photothermal CO_2 utilization. In parallel, embedding TEA/LCA into system design is essential for identifying environmentally favourable pathways and ensuring that CO_2-conversion processes deliver genuine carbon-reduction benefits. Finally, coordinated efforts among policy-makers, industry stakeholders, and the research community are needed to develop regulatory frameworks, certification standards, and demonstration projects, which will reduce technological uncertainty and accelerate the practical implementation of photothermal CO_2 reduction.

Author contributions

Yanlin Liao: conceptualization, data curation, investigation, visualization, writing – original draft, review & editing. Shuangjun Li: writing – original draft, review & editing. Yan Xie: visualization, writing – review & editing. Hao Wen: writing – review & editing. Hao Sun: supervision, visualization, writing – review & editing. Xiangzhou Yuan: supervision, visualization, validation, funding acquisition, writing – original draft, review & editing.

Conflicts of interest

There are no conflicts to declare.

Data availability

No primary research results, software or code have been included and no new data were generated or analysed as part of this review.

Acknowledgements

This work was supported by the National Natural Science Foundation of China (grant number 52476183 and 42377249) and the Start-up Research Fund of Southeast University (grant number RF1028623274). Selected graphics licensed *via* svgrepo.com.

References

1 *Trends in CO_2 - NOAA Global Monitoring Laboratory*, 2025, https://gml.noaa.gov/ccgg/trends/global.html, accessed 2025-09-16.
2 M. Bui, C. S. Adjiman, A. Bardow, E. J. Anthony, A. Boston, S. Brown, P. S. Fennell, S. Fuss, A. Galindo, L. A. Hackett, J. P. Hallett, H. J. Herzog, G. Jackson, J. Kemper, S. Krevor, G. C. Maitland, M. Matuszewski, I. S. Metcalfe, C. Petit, G. Puxty, J. Reimer, D. M. Reiner, E. S. Rubin, S. A. Scott, N. Shah, B. Smit, J. P. M. Trusler, P. Webley, J. Wilcox and N. Mac Dowell, *Energy Environ. Sci.*, 2018, **11**, 1062–1176.
3 O. S. Bushuyev, P. De Luna, C. T. Dinh, L. Tao, G. Saur, J. van de Lagemaat, S. O. Kelley and E. H. Sargent, *Joule*, 2018, **2**, 825–832.
4 R. G. Grim, J. R. Ferrell Iii, Z. Huang, L. Tao and M. G. Resch, *Joule*, 2023, **7**, 1684–1699.
5 D. Kim, S. Bhattacharjee, E. Lam, C. Casadevall, S. Rodriguez-Jimenez and E. Reisner, *Small*, 2024, **20**, e2400057.
6 B. Chang, H. Pang, F. Raziq, S. Wang, K.-W. Huang, J. Ye and H. Zhang, *Energy Environ. Sci.*, 2023, **16**, 4714–4758.
7 J. Hu, Y. Cai, J. Xie, D. Hou, L. Yu and D. Deng, *Chem*, 2024, **10**, 1084–1117.
8 T. Bouwens, S. J. Cobb, C. W. S. Yeung, Y. Liu, G. Martins, I. A. C. Pereira and E. Reisner, *J. Am. Chem. Soc.*, 2025, **147**, 13114–13119.
9 Y. Song, X. Zhang, K. Xie, G. Wang and X. Bao, *Adv. Mater.*, 2019, **31**, e1902033.
10 C. Wang, X. Wu, H. Sun, Z. Xu, C. Xu, X. Wang, M. Li, Y. Wang, Y. Tang, J. Jiang, K. Sun and G. Fu, *Energy Environ. Sci.*, 2025, **18**, 4276–4287.
11 J. Kaur and S. C. Peter, *Angew. Chem., Int. Ed.*, 2025, **64**, e202418708.
12 Y. Xiao, G. Ding, J. Tao, Z. Wang, Z. Chen, L. Chen, L. Shuai and G. Liao, *Nat. Commun.*, 2025, **16**, 7476.
13 Y. Hu, C. Yu, S. Wang, Q. Wang, M. Reinhard, G. Zhang, F. Zhan, H. Wang, D. Skoien, T. Kroll, P. Su, L. Li, A. Chen, G. Liu, H. Lv, D. Sokaras, C. Gao, J. Jiang, Y. Tao and Y. Xiong, *Nat. Catal.*, 2025, **8**, 126–136.
14 Y. Fu, Y. Gao, H. Jia, Y. Zhao, Y. Feng, W. Zhu, F. Zhang, M. D. Argyle and M. Fan, *Green Energy Environ.*, 2025, **10**, 804–812.
15 Y. Cao, R. Guo, M. Ma, Z. Huang and Y. Zhou, *Acta Phys.-Chim. Sin.*, 2024, **40**, 2303029.
16 X. Li, L. Li, X. Chu, X. Liu, G. Chen, Q. Guo, Z. Zhang, M. Wang, S. Wang, A. Tahn, Y. Sun and X. Feng, *Nat. Commun.*, 2024, **15**, 5639.
17 X. Wan, Y. Zhao, Y. Li, J. Ma, Y. Gu, C. Liu, Y. Luo, G. Yang, Y. Cui, D. Liu and Y. Xiong, *Angew. Chem., Int. Ed.*, 2025, **64**, e202505244.
18 Y. Dong, R. Song, Z. Zhang, X. Han, B. Wang, S. Tao, J. Zhao, A. N. Alodhayb, Z. Chen, X. Yi and N. Zhang, *Cell Rep. Phys. Sci.*, 2024, **5**, 102227.
19 J. Sun, W. Sun, L. Wang and G. A. Ozin, *Acc. Mater. Res.*, 2022, **3**, 1260–1271.

This journal is © The Royal Society of Chemistry 2026

Open Access Article. Published on 10 2026. Downloaded on 17.05.26 9:18:50.
This article is licensed under a Creative Commons Attribution-NonCommercial 3.0 Unported Licence.

20 H. Zhang, Z. Wang, X. Luo, J. Lu, S. Peng, Y. Wang and L. Han, *Front. Chem.*, 2019, **7**, 919.
21 X. Cui, Q. Ruan, X. Zhuo, X. Xia, J. Hu, R. Fu, Y. Li, J. Wang and H. Xu, *Chem. Rev.*, 2023, **123**, 6891–6952.
22 M. Hu, Z. Yao and X. Wang, *Ind. Eng. Chem. Res.*, 2017, **56**, 3477–3502.
23 X. Meng, T. Wang, L. Liu, S. Ouyang, P. Li, H. Hu, T. Kako, H. Iwai, A. Tanaka and J. Ye, *Angew. Chem., Int. Ed.*, 2014, **53**, 11478–11482.
24 H. Zhang, T. Wang, J. Wang, H. Liu, T. D. Dao, M. Li, G. Liu, X. Meng, K. Chang, L. Shi, T. Nagao and J. Ye, *Adv. Mater.*, 2016, **28**, 3703–3710.
25 G. Chen, R. Gao, Y. Zhao, Z. Li, G. I. N. Waterhouse, R. Shi, J. Zhao, M. Zhang, L. Shang, G. Sheng, X. Zhang, X. Wen, L. Z. Wu, C. H. Tung and T. Zhang, *Adv. Mater.*, 2018, **30**, 1704663.
26 F. Xu, K. Meng, B. Zhu, H. Liu, J. Xu and J. Yu, *Adv. Funct. Mater.*, 2019, **29**, 1904256.
27 S. Ning, H. Xu, Y. Qi, L. Song, Q. Zhang, S. Ouyang and J. Ye, *ACS Catal.*, 2020, **10**, 4726–4736.
28 H. Wang, S. Fu, B. Shang, S. Jeon, Y. Zhong, N. J. Harmon, C. Choi, E. A. Stach and H. Wang, *Angew. Chem., Int. Ed.*, 2023, **62**, e202305251.
29 M. Guo, Z. Wang, X. Wu, J. Qiu, L. Gu and Z. Yang, *ACS Appl. Energy Mater.*, 2023, **6**, 2863–2876.
30 S. Ren, J. Han, Z. Yang, J. Liang, S. Feng, X. Zhang, J. Xu and J. Zhu, *Angew. Chem., Int. Ed.*, 2024, **64**, e202416376.
31 M. S. Khosrowshahi, H. Mashhadimoslem, H. Shayesteh, G. Singh, E. Khakpour, X. Guan, M. Rahimi, F. Maleki, P. Kumar and A. Vinu, *Adv. Sci.*, 2023, **10**, e2304289.
32 H. Li, Z. Xiao, R. Hao, X. Tan, F. Ye, J. Gu, J. Li, G. Li, J.-J. Zou and D. Wang, *Sep. Purif. Technol.*, 2025, **365**, 132637.
33 C. Choi, F. Zhao, J. L. Hart, Y. Gao, F. Menges, C. L. Rooney, N. J. Harmon, B. Shang, Z. Xu, S. Suo, Q. Sam, J. J. Cha, T. Lian and H. Wang, *Angew. Chem., Int. Ed.*, 2023, **62**, e202302152.
34 D. Mateo, J. Albero and H. García, *Energy Environ. Sci.*, 2017, **10**, 2392–2400.
35 Z. Chen, X. Dong, Z.-X. Sun, X. An, C. Li, S. Liu, J. Shen, C. Wu, J. Wang, Z. Wang, Z. Zhu, Y. Zhou, K. Yu, Y. Ma, J. He, K. Feng, L. He and Z. Hu, *ACS Nano*, 2024, **18**, 19672–19681.
36 X. Wang, L. Garzon-Tovar, A. Rendón-Patiño, D. Mateo and J. Gascon, *Catal. Sci. Technol.*, 2025, **15**, 1814–1824.
37 H. Wang, B. Shang, C. Choi, S. Jeon, Y. Gao, T. Wang, N. J. Harmon, M. Liu, E. A. Stach and H. Wang, *Nano Res.*, 2025, **18**, 94907160.
38 W. Wang, Y. Wang, X. Kong, H. Ning and M. Wu, *Carbon Future*, 2024, **1**, 9200016.
39 X.-L. Lu, X. Rong, C. Zhang and T.-B. Lu, *J. Mater. Chem. A*, 2020, **8**, 10695–10708.
40 N. Syed, J. Huang, Y. Feng, X. Wang and L. Cao, *Front. Chem.*, 2019, **7**, 713.
41 J. Wu, T. Sharifi, Y. Gao, T. Zhang and P. M. Ajayan, *Adv. Mater.*, 2019, **31**, e1804257.
42 E. V. Ramos-Fernandez, A. Rendon-Patiño, D. Mateo, X. Wang, P. Dally, M. Cui, P. Castaño and J. Gascon, *Adv. Energy Mater.*, 2025, **15**, 2405272.
43 Q. Tang, T. Li, W. Tu, H. Wang, Y. Zhou and Z. Zou, *Adv. Funct. Mater.*, 2024, **34**, 2311609.
44 Z. Xie, W. Cheng, H. Luo, Y. Lei and W. Shi, *Adv. Energy Mater.*, 2025, DOI: 10.1002/aenm.202501840.
45 H. Wen, H. Liao, X. Pan, K. Sun, J. Jiang, Y. Liao, X. Yuan and H. Sun, *Carbon Capture Sci. Technol.*, 2025, **16**, 100482.
46 X. Pan, J. Xu, Y. Wang, M. Ma, H. Liao, H. Sun, M. Fan, K. Wang, K. Sun and J. Jiang, *Prog. Nat. Sci.:Mater. Int.*, 2024, **34**, 482–494.
47 C. C. Amoo, Q. Ge, V. Ordomsky and J. Sun, *Adv. Sci.*, 2025, **12**, 2410280.
48 J. Zhou, H. Liu and H. Wang, *Chin. Chem. Lett.*, 2023, **34**, 107420.
49 S. Wang, J. Wang, Y. Wang, X. Sui, S. Wu, W. Dai, Z. Zhang, Z. Ding and J. Long, *ACS Catal.*, 2024, **14**, 10760–10788.
50 E. Gong, S. Ali, C. B. Hiragond, H. S. Kim, N. S. Powar, D. Kim, H. Kim and S.-I. In, *Energy Environ. Sci.*, 2022, **15**, 880–937.
51 S. Chen, Y. Qi, C. Li, K. Domen and F. Zhang, *Joule*, 2018, **2**, 2260–2288.
52 X. Chang, T. Wang and J. Gong, *Energy Environ. Sci.*, 2016, **9**, 2177–2196.
53 K. N. da Silva, S. Shetty, S. Sullivan Allsop, R. Cai, S. Wang, J. Quiroz, M. Chundak, H. L. S. Dos Santos, I. Abdelsalam, F. E. Oropeza, V. A. de la Pena O'Shea, N. Heikkinen, E. Sitta, T. V. Alves, M. Ritala, W. Huo, T. J. A. Slater, S. J. Haigh and P. H. C. Camargo, *ACS Nano*, 2024, **18**, 24391–24403.
54 S. Li, J. Yang, X. Ruan, X. Cui and S. K. Ravi, *Adv. Funct. Mater.*, 2026, **36**, 2503186.
55 L. Zhou, Q. Huang and Y. Xia, *Chem. Rev.*, 2024, **124**, 8597–8619.
56 E. A. Paredes-Salazar, A. Calderón-Cárdenas, E. Herrero and H. Varela, *J. Catal.*, 2024, **432**, 115402.
57 F. Fresno, A. Iglesias-Juez and J. M. Coronado, *Top. Curr. Chem.*, 2023, **381**, 21.
58 H. He, Y. Ren, Y.-H. Zhu, R. Peng, S. Lan, J. Zhou, B. Yang, Y. Si and N. Li, *ACS Catal.*, 2025, **15**, 10480–10520.
59 S. Chen, T. Takata and K. Domen, *Nat. Rev. Mater.*, 2017, **2**, 17050.
60 H. Yang, K. Dai, J. Zhang and G. Dawson, *Chin. J. Catal.*, 2022, **43**, 2111–2140.
61 Z. Wang, C. Li and K. Domen, *Chem. Soc. Rev.*, 2019, **48**, 2109–2125.
62 A. Gelle, T. Jin, L. Garza, G. D. Price, L. V. Besteiro and A. Moores, *Chem. Rev.*, 2020, **120**, 986–1041.
63 D. Mateo, J. L. Cerrillo, S. Durini and J. Gascon, *Chem. Soc. Rev.*, 2021, **50**, 2173–2210.
64 H. Jiang, L. Wang, H. Kaneko, R. Gu, G. Su, L. Li, J. Zhang, H. Song, F. Zhu, A. Yamaguchi, J. Xu, F. Liu, M. Miyauchi, W. Ding and M. Zhong, *Nat. Catal.*, 2023, **6**, 519–530.
65 V. Georgakilas, J. A. Perman, J. Tucek and R. Zboril, *Chem. Rev.*, 2015, **115**, 4744–4822.
66 X. Yu, S. Fan, B. Zhu, S. I. El-Hout, J. Zhang and C. Chen, *Green Energy Environ.*, 2025, **10**, 1377–1436.
67 Y. Shi, Y. Wang, N. Meng and Y. Liao, *Small Methods*, 2024, **8**, e2301554.

Open Access Article. Published on 10 2026. Downloaded on 17.05.26 9:18:50.
This article is licensed under a Creative Commons Attribution-NonCommercial 3.0 Unported Licence.

68 H. Wang, Q. Li, J. Chen and H. Jia, *J. Mater. Chem. A*, 2024, **12**, 15803–15813.
69 W. Wang, D. Xu, B. Cheng, J. Yu and C. Jiang, *J. Mater. Chem. A*, 2017, **5**, 5020–5029.
70 S. Fang and Y. H. Hu, *Chem. Soc. Rev.*, 2022, **51**, 3609–3647.
71 F. Yang, X. Liu, C. Xing, Z. Chen, L. Zhao, X. Liu, W. Gao, L. Zhu, H. Liu and W. Zhou, *Adv. Sci.*, 2024, **11**, e2406828.
72 Z. Wang, X. Dong, Z. Sun, Y. Zhou, S. Liu, S. Qian, Z. Chen, X. An, K. Nie, B. Yan, Z. Zhu, X. Zhang, C. Li, K. Feng, Z. Hu and L. He, *ACS Appl. Mater. Interfaces*, 2025, **17**, 32413–32422.
73 J. Liu, Z. Huang, X. Zheng, M. S. Nasir, D. Wang, P. Wang, J. Li, Y. Li, L. Zhu, X. Wang, Z. Huang and B. Zhou, *Angew. Chem., Int. Ed.*, 2025, **64**, e202511886.
74 Q. Ma, D. Li, F. Ren, W. Gao, R. Song, Z. Li and C. Li, *Angew. Chem., Int. Ed.*, 2025, **64**, e202506322.
75 S. Liu, X. Wang, Y. Chen, Y. Li, Y. Wei, T. Shao, J. Ma, W. Jiang, J. Xu, Y. Dong, C. Wang, H. Liu, C. Gao and Y. Xiong, *Adv. Mater.*, 2024, **36**, 2311957.
76 X. Kang, Z. He, F. Wang, Y. Liu and L. Guo, *Adv. Funct. Mater.*, 2024, **35**, 2419802.
77 Y. Mochizuki, J. Bud, E. Byambajav and N. Tsubouchi, *Carbon Resour. Convers.*, 2025, **8**, 100237.
78 P. Guo, R. Xue, Q. Zou, X. Ma, C. Su, Z. Zeng and L. Li, *Energy Environ. Mater.*, 2025, DOI: 10.1002/eem2.70140.
79 X. Yuan, J. G. Lee, H. Yun, S. Deng, Y. J. Kim, J. E. Lee, S. K. Kwak and K. B. Lee, *Chem. Eng. J.*, 2020, **397**, 125350.
80 X. Pan, H. Sun, M. Ma, H. Liao, G. Zhan, K. Wang, M. Fan, J. Xu, L. Ding, K. Sun and J. Jiang, *Biochar*, 2024, **6**, 93.
81 S. Ning, X. Wu, H. Song, X. Ma, S. Yue, S. Zhang, L. Tang, R. Liu, X. Yin, S. Ouyang and J. Ye, *J. Am. Chem. Soc.*, 2025, **148**, 1728–1740.
82 X. Liu, C. Wang, C. Chen, Z. Pan, C. Gao, W. Lai, J. Zhao, T. Tian and W. Xiao, *Coord. Chem. Rev.*, 2025, **544**, 216927.
83 M. Xu, X. Hu, S. Wang, J. Yu, D. Zhu and J. Wang, *J. Catal.*, 2019, **377**, 652–661.
84 D. Mateo, J. Albero and H. García, *Appl. Catal., B*, 2018, **224**, 563–571.
85 R. Feng, M. Guo, Z. Yang, J. Qiu, Z. Wang and Y. Zhao, *Carbon*, 2024, **224**, 119079.
86 M. Guo, J. Liu, J. Qiu, Z. Wang and Z. Yang, *Gas Sci. Eng.*, 2024, **128**, 205383.
87 Z. Wang, Z. Yang, J. He, Y. Wang, M. Guo, X. Du, J. Ran, Z. Zhang and H. Arandiyan, *Carbon Energy*, 2025, **7**, e70032.
88 R. Fang, Z. Yang, M. Guo, Z. Wang, J. Qiu, J. Ran and C. Xue, *Appl. Surf. Sci.*, 2024, **656**, 159712.
89 P. Zhu, M. Geng, S. Qin, H. Cao, Z. He, X. Gao and C. Wang, *Surf. Interfaces*, 2024, **46**, 104032.
90 J. Ma, J. Yu, G. Chen, Y. Bai, S. Liu, Y. Hu, M. Al-Mamun, Y. Wang, W. Gong, D. Liu, Y. Li, R. Long, H. Zhao and Y. Xiong, *Adv. Mater.*, 2023, **35**, 2302537.
91 Z. Xia, J. Zhai, L. Lin, X. Chen, C. Xue, S. Jia, J. Jiao, M. Dong, W. Han, X. Zheng, T. Xue, H. Wu and B. Han, *Chem. Sci.*, 2025, **16**, 13382–13389.
92 R. Hu, L. Chu, J. Zhang, X. a. Li and W. Huang, *J. Power Sources*, 2017, **361**, 259–275.
93 S. Fu, E. Jin, H. Hanayama, W. Zheng, H. Zhang, L. Di Virgilio, M. A. Addicoat, M. Mezger, A. Narita, M. Bonn, K. Mullen and H. I. Wang, *J. Am. Chem. Soc.*, 2022, **144**, 7489–7496.
94 L. Junfeng, W. Shengda, Z. Fan, Y. Bowen, D. Pingwu, C. Chuanfeng, Z. Yaping and Z. Daoben, *Sci. Adv.*, 2022, **8**, eade4692.
95 R. Lamba, Y. Yukta, J. Mondal, R. Kumar, B. Pani and B. Singh, *ACS Appl. Bio Mater.*, 2024, **7**, 2086–2127.
96 J. Lu, Z. Chen, Y. Shen, H. Yuan, X. Sun, J. Hou, F. Guo, C. Li and W. Shi, *J. Colloid Interface Sci.*, 2024, **670**, 428–438.
97 W. Hou, H. Guo, M. Wu and L. Wang, *ACS Nano*, 2023, **17**, 20560–20569.
98 L. Q. Yu, R. T. Guo, C. Xia, S. H. Guo, J. S. Yan and Y. F. Liu, *Small*, 2025, **21**, e2409901.
99 X. Zeng, H. Chen, Y. Liu, W. Fang, Z. Huang and L. Zhao, *J. Colloid Interface Sci.*, 2025, **686**, 733–742.
100 W. Zhang, X. Zhao, Q. Liu, M. Zhang, N. Xi, C. Cui, X. Yu, X. Wang, Y. Wang, H. Liu and Y. Sang, *Nano Energy*, 2023, **116**, 108806.
101 Q. Hao, Z. Li, Y. Shi, R. Li, Y. Li, L. Wang, H. Yuan, S. Ouyang and T. Zhang, *Angew. Chem., Int. Ed.*, 2023, **62**, e202312808.
102 L. Gan, J. Zhou, F. Ke, H. Gu, D. Li, Z. Hu, Q. Sun and X. Guo, *NPG Asia Mater.*, 2012, **4**, e31.
103 H. Szalad, L. Peng, A. Primo, J. Albero and H. García, *Chem. Commun.*, 2021, **57**, 10075–10078.
104 Y. Xiao, H. Guo, M. Li, J. He, X. Xu, S. Liu, L. Wang and T. D. James, *Coord. Chem. Rev.*, 2025, **527**, 216378.
105 M. Kohei, I. Juntaro, K. Hideo, H. Yuhei, Y. Satoshi, D. N. Futabaa, Y. Motoo and H. Kenji, *Proc. Natl. Acad. Sci. U. S. A.*, 2009, **106**, 6044–6047.
106 A. Pasciak, R. Marin, L. Abiven, A. Pilch-Wrobel, M. Misiak, W. Xu, K. Prorok, O. Bezkrovnyi, L. Marciniak, C. Chaneac, F. Gazeau, R. Bazzi, S. Roux, B. Viana, V. P. Lehto, D. Jaque and A. Bednarkiewicz, *ACS Appl. Mater. Interfaces*, 2022, **14**, 33555–33566.
107 S. Balou, P. Shandilya and A. Priye, *Front. Chem.*, 2022, **10**, 1023602.
108 L. Liu, X. Wang, H. Jin, J. Wang and Q. Li, *Adv. Sustainable Syst.*, 2024, **9**, 2400757.
109 I. S. Khan, D. Mateo, G. Shterk, T. Shoinkhorova, D. Poloneeva, L. Garzon-Tovar and J. Gascon, *Angew. Chem., Int. Ed.*, 2021, **60**, 26476–26482.
110 X. Shang, Y. Gu, Y. Zhou, Z. Lian, M. Yu, J. Ding and Q. Zhong, *Adv. Funct. Mater.*, 2026, **36**, e12566.
111 J. Xu, H. Sun, X. Pan, K. Wang, S. Zhang, M. Ma, W. Tan, H. Liao, Y. Wang, H. Yuan, K. Sun and J. Jiang, *Biomass Bioenergy*, 2025, **195**, 107710.
112 Z. X. Sun, C. Zhou, Z. Chen, Y. Zeng, T. Sun, X. Dong, L. Yang, X. Wang, Q. Wu, H. Huang, L. He and Z. Hu, *Angew. Chem., Int. Ed.*, 2025, **64**, e202508090.
113 X. Fan, D. Li, Y. Shu, Y. Feng and F. Li, *ACS Catal.*, 2024, **14**, 12991–13014.
114 X. Zhao, I. A. Khan, M. B. Asif and Z. Zhang, *Appl. Catal., B*, 2026, **381**, 125877.

This journal is © The Royal Society of Chemistry 2026

Open Access Article. Published on 10 2026. Downloaded on 17.05.26 9:18:50.
This article is licensed under a Creative Commons Attribution-NonCommercial 3.0 Unported Licence.

115 X. Zhang, J. Guo, L. Huang, S. Li, X. Zhou, Y. Zhang, Q. Xie, S. Mo, B. Li and J. Li, *Sep. Purif. Technol.*, 2025, **360**, 131047.
116 X. Zou, D. Liu, Z. Ou, X. Liu and X. Yang, *J. Alloys Compd.*, 2025, **1047**, 185052.
117 S. Mo, X. Zhao, S. Li, L. Huang, X. Zhao, Q. Ren, M. Zhang, R. Peng, Y. Zhang, X. Zhou, Y. Fan, Q. Xie, Y. Guo, D. Ye and Y. Chen, *Angew. Chem., Int. Ed.*, 2023, **62**, e202313868.
118 X. Dong, Z. Zhu, Z. Chen, Z. Sun, S. Qian, Z. Wang, Y. Zhou, K. Nie, S. Liu, Z. Li, M. Xiao, J. Zhang, B. Yan, Y. Cheng, C. Li, X. Zhang, X. An, K. Feng, Z. Hu and L. He, *ACS Nano*, 2025, **19**, 25403–25412.
119 Y. Qi, J. Jiang, X. Liang, S. Ouyang, W. Mi, S. Ning, L. Zhao and J. Ye, *Adv. Funct. Mater.*, 2021, **31**, 2100908.
120 X. Song, G. Li, W. Zhou, Y. Wu, X. Liu, Z. Zhu, P. Huo and M. Wang, *J. Colloid Interface Sci.*, 2024, **664**, 868–881.
121 J. Zhao, Y. Bai, X. Liang, T. Wang and C. Wang, *J. CO_2 Util.*, 2021, **49**, 101562.
122 Z. Guo, B. Shen, Z. Jiang, N. Wu and Y. You, *Ind. Eng. Chem. Res.*, 2024, **63**, 18931–18939.
123 P. Li, L. Liu, W. An, H. Wang, H. Guo, Y. Liang and W. Cui, *Appl. Catal., B*, 2020, **266**, 118618.
124 P. Wang, Q. Jiang, X. Li, X. Wang and J. Hu, *Mol. Catal.*, 2025, **570**, 114686.
125 J. Wang, Z. Hu, N. Ullah, Y. Wei, C. Zhuang, C. He, C. Liu, Y. Cao, F. Meng, W. Ye and H. Jing, *Chem. Eng. J.*, 2025, **507**, 160633.
126 H. Cui, Y. Guo, L. Guo, L. Wang, Z. Zhou and Z. Peng, *J. Mater. Chem. A*, 2018, **6**, 18782–18793.
127 S. Zhi, Q. Dai, H. Wang, D. Wu, L. Zhao, C. Hu and L. Dai, *ACS Nano*, 2025, **19**, 29860–29897.
128 Y. Xia, B. Cheng, J. Fan, J. Yu and G. Liu, *Sci. China Mater.*, 2020, **63**, 552–565.
129 L. An, S. Liu, L. Wang, J. Wu, Z. Wu, C. Ma, Q. Yu and X. Hu, *Ind. Eng. Chem. Res.*, 2019, **58**, 3349–3358.
130 X. Pan, C. Wang, B. Li, M. Ma, H. Sun, G. Zhan, K. Wang, M. Fan, L. Ding, G. Fu, K. Sun and J. Jiang, *Adv. Powder Mater.*, 2025, **4**, 100259.
131 W. Ni, Z. Liu, Y. Zhang, C. Ma, H. Deng, S. Zhang and S. Wang, *Adv. Mater.*, 2021, **33**, e2003238.
132 S. Mao, C. Wang and Y. Wang, *J. Catal.*, 2019, **375**, 456–465.
133 T. Wang, F. Chen, H. An, K. Chen and J. Gao, *J. Solid State Chem.*, 2024, **332**, 124570.
134 H. Yu, M. Dai, J. Zhang, W. Chen, Q. Jin, S. Wang and Z. He, *Small*, 2023, **19**, e2205767.
135 Y. Yusran, S. Qiu and Q. Fang, *EnergyChem*, 2025, **7**, 100170.
136 Y. Ye and L. Dai, *J. Mater. Chem.*, 2012, **22**, 24224.
137 C. K. Ku, P. H. Wu, C. C. Chung, C. C. Chen, K. J. Tsai, H. M. Chen, Y. C. Chang, C. H. Chuang, C. Y. Wei, C. Y. Wen, T. Y. Lin, H. L. Chen, Y. S. Wang, Z. Y. Lee, J. R. Chang, C. W. Luo, D. Y. Wang, B. J. Hwang and C. W. Chen, *Adv. Energy Mater.*, 2019, **9**, 1901022.
138 L. Wang, H. Tan, L. Zhang, B. Cheng and J. Yu, *Chem. Eng. J.*, 2021, **411**, 128501.
139 Y. Wang, J. Ding, Q. Yin, C. Zhang, Y. Zeng, S. Xu, Q. Liang, M. Zhou and Z. Li, *J. Alloys Compd.*, 2024, **996**, 174761.
140 H. Yang, Z. Wang, J. Zhang, K. Dai and J. Low, *J. Materiomics*, 2025, **11**, 100996.
141 Y. Zhou, P. Zheng, F. Wang, F. Gu, W. Xu, Q. Lu, T. Zhu, Z. Zhong, G. Xu and F. Su, *Nano Res.*, 2023, **17**, 2283–2290.
142 Y. Qi, S. Li, T. Bao, P. She, H. Rao and J.-s. Qin, *Appl. Catal., B*, 2024, **357**, 124299.
143 L. Sun, Z. Zhang, J. Bian, F. Bai, H. Su, Z. Li, J. Xie, R. Xu, J. Sun, L. Bai, C. Chen, Y. Han, J. Tang and L. Jing, *Adv. Mater.*, 2023, **35**, e2300064.
144 Y. Wang, X. Shang, J. Shen, Z. Zhang, D. Wang, J. Lin, J. C. S. Wu, X. Fu, X. Wang and C. Li, *Nat. Commun.*, 2020, **11**, 3043.
145 C. Song, Z. Wang, Z. Yin, D. Xiao and D. Ma, *Chem Catal.*, 2022, **2**, 52–83.
146 W. Han, Y. Chen, Y. Jiao, S. Liang, W. Li and G. Tian, *J. Mater. Chem. A*, 2022, **10**, 17642–17651.
147 Z. Yang, Z.-Y. Wu, Z. Lin, T. Liu, L. Ding, W. Zhai, Z. Chen, Y. Jiang, J. Li, S. Ren, Z. Lin, W. Liu, J. Feng, X. Zhang, W. Li, Y. Yu, B. Zhu, F. Ding, Z. Li and J. Zhu, *Nat. Commun.*, 2024, **15**, 7599.
148 M. Meena, S. Shubham, K. Paritosh, N. Pareek and V. Vivekanand, *Bioresour. Technol.*, 2021, **340**, 125642.
149 Z. Yang, Z. Y. Wu, Z. Lin, T. Liu, L. Ding, W. Zhai, Z. Chen, Y. Jiang, J. Li, S. Ren, Z. Lin, W. Liu, J. Feng, X. Zhang, W. Li, Y. Yu, B. Zhu, F. Ding, Z. Li and J. Zhu, *Nat. Commun.*, 2024, **15**, 7599.
150 F. Alfarra, H. K. Ozcan, P. Cihan, A. Ongen, S. Y. Guvenc and M. N. Ciner, *Environ. Monit. Assess.*, 2024, **196**, 309.
151 V. Sharma, M. L. Tsai, C. W. Chen, P. P. Sun, P. Nargotra and C. D. Dong, *Sci. Total Environ.*, 2023, **886**, 163972.
152 G. C. Umenweke, I. C. Afolabi, E. I. Epelle and J. A. Okolie, *Bioresour. Technol. Rep.*, 2022, **17**, 100976.
153 S. Li, X. Yuan, S. Deng, L. Zhao and K. B. Lee, *Renewable Sustainable Energy Rev.*, 2021, **152**, 111708.
154 J. X. Tee, A. Selvarajoo and S. K. Arumugasamy, *J. Environ. Chem. Eng.*, 2022, **10**, 107640.
155 K. Jeyasubramanian, B. Thangagiri, A. Sakthivel, J. Dhaveethu Raja, S. Seenivasan, P. Vallinayagam, D. Madhavan, S. Malathi Devi and B. Rathika, *Fuel*, 2021, **292**, 120243.
156 Y. Song, Z. Huang, M. Jin, Z. Liu, X. Wang, C. Hou, X. Zhang, Z. Shen and Y. Zhang, *J. Anal. Appl. Pyrolysis*, 2024, **181**, 106596.
157 B. Pomeroy, M. Grilc and B. Likozar, *Renewable Sustainable Energy Rev.*, 2022, **153**, 111748.
158 K. Manatura, B. Chalermsinsuwan, N. Kaewtrakulchai, E. E. Kwon and W. H. Chen, *Bioresour. Technol.*, 2023, **369**, 128504.
159 S. Li, Z. Huang, Y. Li, S. Deng and X. E. Cao, *Energy AI*, 2025, **20**, 100477.
160 X. Yuan, M. Suvarna, S. Low, P. D. Dissanayake, K. B. Lee, J. Li, X. Wang and Y. S. Ok, *Environ. Sci. Technol.*, 2021, **55**, 11925–11936.
161 S. Li, Y. Xie, S. Deng and X. Yuan, *Acc. Mater. Res.*, 2025, **6**, 1319–1331.
162 V. B. Borugadda, G. Kamath and A. K. Dalai, *Energy*, 2020, **195**, 116985.
163 X. Ding, W. Liu, J. Zhao, L. Wang and Z. Zou, *Adv. Mater.*, 2025, **37**, e2312093.

Open Access Article. Published on 10 2026. Downloaded on 17.05.26 9:18:50. This article is licensed under a Creative Commons Attribution-NonCommercial 3.0 Unported Licence.

164 A. Kumar, R. Wang, K. A. Orton, K. M. Van Allsburg, C. Mukarakate, E. C. Wegener, Q. Wu, S. E. Habas, K. Z. Pupek, J. A. Libera and F. G. Baddour, *Catal. Sci. Technol.*, 2023, **13**, 4941–4954.
165 F. Feizi, F. Reguyal, N. Antoniou, A. Zabaniotou and A. K. Sarmah, *Sci. Total Environ.*, 2020, **739**, 139855.
166 M. Cavali, N. Libardi Junior, R. d. A. Mohedano, P. Belli Filho, R. H. R. da Costa and A. B. de Castilhos Junior, *Sci. Total Environ.*, 2022, **822**, 153614.
167 T. Haeldermans, L. Campion, T. Kuppens, K. Vanreppelen, A. Cuypers and S. Schreurs, *Bioresour. Technol.*, 2020, **318**, 124083.
168 M. Nematian, C. Keske and J. N. Ng'ombe, *Waste Manage.*, 2021, **135**, 467–477.
169 M. Zbair, H. Ait Ahsaine and Z. Anfar, *J. Cleaner Prod.*, 2018, **202**, 571–581.
170 P. Chakraborty, S. Banerjee, S. Kumar, S. Sadhukhan and G. Halder, *Process Saf. Environ. Prot.*, 2018, **118**, 10–23.
171 K. Ulonska, A. König, M. Klatt, A. Mitsos and J. Viell, *Ind. Eng. Chem. Res.*, 2018, **57**, 6980–6991.
172 B. Wu, R. Lin, R. O'Shea, C. Deng, K. Rajendran and J. D. Murphy, *Renewable Sustainable Energy Rev.*, 2021, **135**, 110371.
173 H. Bamdad, K. Hawboldt and S. MacQuarrie, *Energy Fuels*, 2018, **32**, 11742–11748.
174 C. Wurzer and O. Mašek, *Bioresour. Technol.*, 2021, **321**, 124473.
175 S.-y. Wang, Y.-k. Tang, C. Chen, J.-t. Wu, Z. Huang, Y.-y. Mo, K.-x. Zhang and J.-b. Chen, *Bioresour. Technol.*, 2015, **186**, 360–364.
176 M. A. Ilgin and S. M. Gupta, *J. Environ. Manage.*, 2010, **91**, 563–591.
177 F. J. Lozano and R. Lozano, *J. Cleaner Prod.*, 2018, **172**, 4162–4169.
178 X. Li and E. Mupondwa, *Sci. Total Environ.*, 2014, **481**, 17–26.
179 M. Belluati, S. Tabasso, E. Calcio Gaudino, G. Cravotto and M. Manzoli, *Green Chem.*, 2024, **26**, 8642–8668.
180 S. Li, Z. Du, J. Wang, H. Wang, X. E. Cao, R. Chen, Y. Pang, S. Deng, O. Mašek, X. Yuan and K. B. Lee, *Carbon Res.*, 2025, **4**, 43.
181 B. Dutta and V. Raghavan, *Int. J. Energy Environ. Eng.*, 2014, **5**, 106.
182 R. Ibarrola, S. Shackley and J. Hammond, *Waste Manage.*, 2012, **32**, 859–868.
183 A. C. M. Loy, H. Alhazmi, S. S. M. Lock, C. L. Yiin, K. W. Cheah, B. L. F. Chin, B. S. How and S. Yusup, *Bioresour. Technol.*, 2021, **341**, 125796.
184 B. Cao, D. Jiang, Y. Zheng, P. Fatemeh Rupani, C. Yuan, Y. Hu, H. Chen, C. Li, X. Hu, S. Wang, J. Yuan and A. Abomohra, *Fuel*, 2022, **330**, 125476.
185 C. Gai, Y. Tao, N. Peng, X. Dou and Z. Liu, *J. Anal. Appl. Pyrolysis*, 2025, **186**, 106918.
186 I. Kozyatnyk, D. M. M. Yacout, J. Van Caneghem and S. Jansson, *Bioresour. Technol.*, 2020, **302**, 122866.
187 F. Cheng, M. D. Porter and L. M. Colosi, *Energy Convers. Manage.*, 2020, **203**, 112252.
188 F. Cheng, H. Luo and L. M. Colosi, *Energy Convers. Manage.*, 2020, **223**, 113258.
189 H. Liao, C. Wang, X. Pan, H. Sun, Y. Liao, M. Ma, G. Zhan, M. Fan, L. Ding, J. Xu, Y. Wang, K. Sun, X. Yuan and J. Jiang, *Carbon Energy*, 2026, DOI: 10.1002/cey2.70165.
190 M. Fang, Z. Huang, M. Wang, Z. Wang, X. Feng, J. Ma, L. Dai, Y. Zhu and L. Jiang, *Nat. Commun.*, 2025, **17**, 984.
191 Y. Yang, F. Wang, W. Lyu, D. Tang, D. Chen, X. Zhao, R. Fang and Y. Li, *Angew. Chem., Int. Ed.*, 2025, **64**, e202509855.
192 Y. Li, X. Bai, D. Yuan, C. Yu, X. San, Y. Guo, L. Zhang and J. Ye, *Nat. Commun.*, 2023, **14**, 3171.

 This journal is © The Royal Society of Chemistry 2026